A sleep-active neuron can promote survival while sleep behavior is disturbed

Inka Busack[1], Henrik Bringmann[1]*

[1] BIOTEC, Technical University Dresden, Germany

*Corresponding author: henrik.bringmann@tu-dresden.de

Abstract

Sleep is controlled by neurons that induce a state of behavioral quiescence and physiological restoration. It is not known, however, how sleep neurons link sleep behavior and stress survival. In *Caenorhabditis elegans*, the sleep-active RIS neuron induces sleep behavior and promotes survival of stressful conditions. Sleep-active neurons such as RIS might hypothetically promote survival primarily by causing sleep behavior and associated conservation of energy. Alternatively, RIS might provide a survival benefit that does not depend on behavioral sleep. To probe these hypotheses, we tested how activity of the sleep-active RIS neuron in *Caenorhabditis elegans* controls sleep behavior and survival during larval starvation. To manipulate the activity of RIS, we expressed constitutively active potassium channel (*twk-18gf* and *egl-23gf*) or sodium channel (*unc-58gf*) mutant alleles in this neuron. Low levels of *unc-58gf* expression in RIS increased RIS calcium transients and sleep. High levels of *unc-58gf* expression in RIS elevated baseline calcium activity and inhibited calcium activation transients, thus locking RIS activity at a high but constant level. This manipulation caused a nearly complete loss of sleep behavior but increased survival. Long-term optogenetic activation also caused constantly elevated RIS activity and a small trend towards increased survival. Disturbing sleep by lethal blue-light stimulation also overactivated RIS, which again increased survival. FLP-11 neuropeptides were important for both, induction of sleep behavior and starvation survival, suggesting that FLP-11 might have divergent roles downstream of RIS. These results indicate that promotion of sleep behavior and survival are separable functions of RIS. These two functions may normally be coupled but can be uncoupled during conditions of strong RIS activation or when sleep behavior is impaired. Through this uncoupling, RIS can provide survival benefits under conditions when behavioral sleep is disturbed. Promoting survival in the face of impaired sleep might be a general function of sleep neurons.

Author Summary

The sleep neuron RIS in *Caenorhabditis elegans* is required to induce sleep behavior and to promote survival. Here we show that RIS can provide survival benefits even when sleep is disturbed.

Introduction

Sleep is defined by behavioral inactivity and reduced responsiveness [1]. It is a physiological state that conserves and allocates energy, promotes restorative processes, and is important for brain and cognitive functions [2-4]. Sleep disorders and deviations from the normal sleep amount are widespread in modern societies and pose an unresolved medical and economical problem [5-7].

Sleep is found in most animals ranging from cnidarians to humans. Central to the induction of sleep in all species are so-called sleep-active neurons that activate to inhibit wakefulness behavioral circuits and thus cause sleep behavior [8, 9]. *C. elegans* has a small and invariant nervous system and sleep is controlled by relatively few neurons. RIS is a GABAergic and peptidergic interneuron that activates during sleep, and its ablation virtually abolishes sleep behavior during molting of developing larvae, in arrested larvae, and in adults following cellular stress [10-21]. Optogenetic manipulations showed that acute activation of RIS inhibits wakefulness activity such as feeding and locomotion [10, 15], whereas inactivation of RIS inhibits sleep [12, 18, 22, 23]. RIS is important for survival during starvation and after wounding [12, 18, 24]. This neuron counteracts aging phenotype progression during starvation-induced arrest [12]. It supports the protective transcriptional response that underlies the arrest, and promotes the activity of the FOXO transcription factor DAF-16, which is required for survival [24-26]. Thus, RIS is a sleep-active neuron that is crucial for *C. elegans* sleep and stress survival.

Little is known about how sleep-active neurons such as RIS link sleep behavior and survival. Different hypotheses are conceivable. For example, sleep-active neurons might promote survival by reducing behavioral activities during sleep, thus conserving and allocating energy or optimizing behavior [27, 28]. The close association of sleep and physiological benefits has suggested a causal relationship. For example, memory and information processing are thought to be improved in the human brain during sleep when information inputs are blocked [29, 30], and energy is conserved by reduced behavioral activity [28]. A less explored additional hypothesis is that sleep-active neurons provide benefits during sleep, but independently of sleep behavior. According to this hypothesis,

sleep-active neurons have two parallel functions. The first is to induce sleep behavior, and the second is to promote survival. This hypothesis implies that physiological benefits of sleep-active neuron functions can be exerted also when sleep behavior is impaired.

In order to find out how RIS links sleep and survival, we manipulated RIS activity through transgenic expression of ion channel mutants in RIS. By strongly expressing *unc-58gf* in RIS, we achieved an overall increase of RIS activity that was caused by constantly elevated baseline calcium activity in RIS. RIS appeared to be locked at this higher activity level, as it was not able to activate further upon stimulation. Survival was increased in this strain, but sleep behavior was almost completely lacking. The sleep loss phenotype included a lack of dampening of the activity of interneurons, sensory neurons and muscles that is typical for normal sleep. Thus, strong expression of RIS led to an apparent uncoupling of sleep behavior and survival. Long-term optogenetic activation also generated constantly increased calcium activity and a small trend towards increased survival. Stimulation with blue light disturbed sleep and increased RIS activation, which in turn extended survival. Finally, we find that RIS promotes sleep behavior and promotes survival through FLP-11 neuropeptides.

RIS hence appears to be able to promote survival independently of sleep behavior, indicating that promotion of sleep behavior and survival are separable functions of RIS that are normally coupled during sleep but that can be uncoupled. Uncoupling appears to occur during conditions of stimulation that disturb sleep and increase RIS activity. This suggests that an important function of RIS overactivation is to promote survival not only during normal sleep, but also and in particular when sleep behavior is disturbed. Sleep-active neurons might generally function to promote survival both during normal sleep and even more so when sleep behavior is disturbed.

Results

Generation of a strain set for controlling RIS activity

100

101 We set out to control RIS activity to study sleep and survival during L1 arrest. For this
102 study, we generated strains that express constitutively active ion channels with different
103 ion permeability and expression levels in RIS. To constitutively inactivate RIS, we
104 expressed potassium channels that carry mutations that cause potassium leak currents using
105 the *flp-11* promotor that is strong and highly specific for RIS [11, 17, 31]. We used two
106 different *egl-23* channel mutations to achieve different strengths of inactivation of RIS
107 (*RIS::egl-23gf(weak)* expresses *egl-23(L229N)* in RIS, *RIS::egl-23gf(strong)* expresses
108 *egl-23(A383V)* in RIS) [32]. To create a strong tool for RIS inhibition, we expressed a *twk-*
109 *18* mutant allele that is known to cause a very strong potassium current (*RIS::twk-18gf*
110 expresses *twk-18(e1913)* in RIS) [33]. In all three strains, the channel genes were knocked
111 into the endogenous *flp-11* locus behind the *flp-11* gene to generate operons that express
112 both *flp-11* and the mutant ion channel. All fusion proteins localized to the cell membrane
113 of RIS (Fig 1A-D).

114

115 To constitutively over activate RIS, we used an unusual K2P channel mutant that is
116 permeable to sodium [32] (Thomas Boulin, personal communication). We expressed the
117 ion channel mutant in RIS (*unc-58(L428F),* Fig S1A) tagged with mKate2 at either a lower
118 or a higher level in RIS. The different expression levels were achieved by generating two
119 different expression loci for the channel in the genome. To achieve a strong expression of
120 the *unc-58(L428F)* channel (*RIS::unc-58gf(strong)*), we turned the endogenous *flp-11*
121 locus into an operon as above. To achieve a weaker expression of the channel (*RIS::unc-*
122 *58gf(weak)*), we expressed mKate2-tagged *unc-58(L428F)* from a single-copy knock-in
123 locus on chromosome III [34], which contained only a minimal *flp-11* promoter and 3'
124 UTR [11] (Fig 1 E-H). Fluorescent imaging after two days of L1 arrest showed that the
125 stronger strain expressed at about double the level of the weaker strain and in both
126 transgenes, the channel was expressed prominently in RIS and was targeted to the cell
127 membrane (Fig 1E-H, S1). Even after 21 days of arrest, mKate2-tagged *unc-58(L428F)*
128 expression could be detected in the strong strain indicating that the sodium channel mutant
129 is properly folded and targeted to the plasma membrane across the entire arrest (FigS1E).

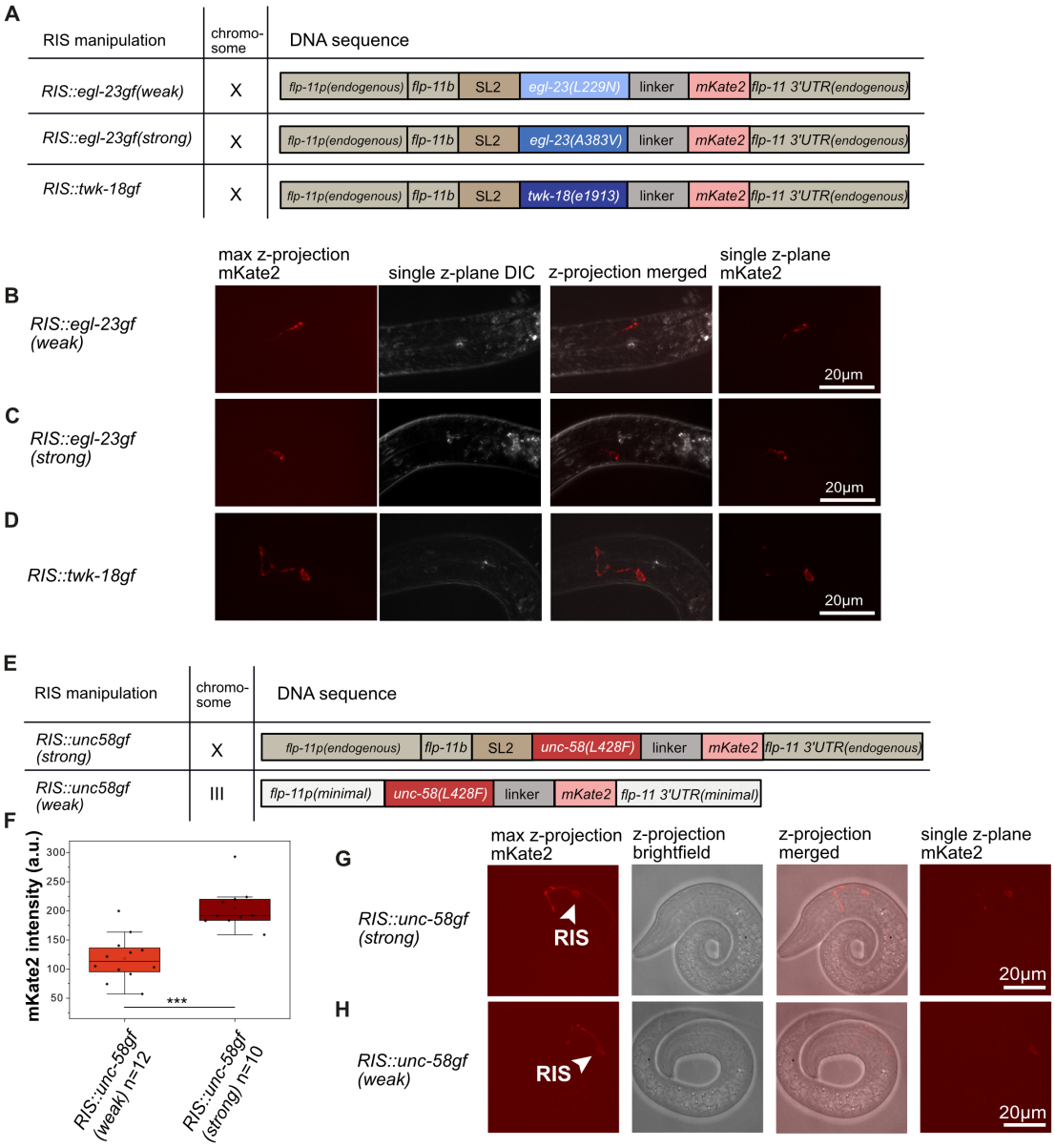

Fig. 1 – Strains expressing ion channel mutants in RIS

A) Scheme of the genetic design of the different RIS potassium channel mutant transgenes.

B-D) Localization and expression of mKate2, which is translationally fused to the ion channels, in the different inactivation strains.

E) Schematic representation of the genetic design of the RIS sodium channel mutant transgenes.

138 F) Quantification of the expression levels of UNC-58gf::mKate2 in the two RIS
139 overactivation strains. ***p<0.001, Welch test.
140 G) Localization and expression of the strong overactivation strain (*RIS::unc-*
141 *58gf(strong)*).
142 H) Localization and expression of the weak overactivation strain (*RIS::unc-58gf(weak)*).
143
144
145 ***RIS::unc-58gf(strong)* promotes survival of L1 arrest**
146
147 Previous studies have shown that RIS is required for survival during larval arrest and
148 following wounding of the adult [12, 18, 35]. RIS activity might act by controlling the gene
149 expression changes that underly the physiological adaptation to stress during starvation
150 [24]. We first confirmed that gene expression changes depend on RIS activity [24]. For
151 this analysis, we compared the gene expression profiles of *RIS::unc-58gf(strong)* and
152 *RIS::twk-18gf* during L1. *RIS::twk-18gf* is more similar to *aptf-1(-)*, which causes loss of
153 RIS function [10, 24]. *RIS::unc-58gf(strong)* and *RIS::twk-18gf* displayed opposing gene
154 expression changes compared with wild type (Figure 2A). This comparison confirms the
155 notion that activation and inactivation of RIS have opposing effects on gene expression
156 [24]. These data support the idea that the expression of *twk-18gf* and *unc-58gf* in RIS cause
157 loss-of-function and gain-of-function gene expression phenotypes of RIS, respectively
158 [24].
159
160 To get an understanding of the role of RIS activation on survival, we investigated how the
161 different RIS-expressed ion channels affect survival in arrested L1 larval worms. For this
162 experiment, we kept arrested L1 larvae as liquid culture, as this allowed for a higher
163 number of animals to be processed. We regularly took a sample of the larvae from the
164 liquid culture and measured two different readouts. We first measured starvation survival
165 by scoring the fraction of animals that had died and secondly, we scored the ability of
166 starved animals to recover and develop to the adult stage after refeeding [12, 23, 24, 36].
167 *RIS::twk-18gf* larvae showed strongly reduced starvation survival by about half compared
168 to the wild type. *egl-23(strong)* resulted in a more moderate yet significant starvation

169 survival reduction of approximately 21%. Weak inactivation by *egl-23(weak)* or
170 overactivation by *unc-58gf(weak)* of RIS activity did not significantly change starvation
171 survival. Strong RIS overactivation by *unc-58gf(strong)* had an increased starvation
172 survival of around 19% compared to wild type (Fig 2B). These results are in accordance
173 with previous reports and the expected changes caused by the ion channel transgenes [12,
174 24, 32, 33]. The recovery upon refeeding matched the survival curves (Fig 2C). To test
175 whether this survival-extending effect was caused by *unc-58gf* expression in RIS, we
176 measured survival of *RIS::unc-58gf(strong)* in the *aptf-1(-)* background, in which
177 expression in RIS is abolished (Fig S1G). In the combined *RIS::unc-58gf(strong); aptf-1(-*
178 *)* strain starvation survival was extremely shortened compared with wild type (Fig S2) and
179 was similar to *aptf-1(-)* [12] or *RIS::twk-18gf* (Fig 2B), indicating that the starvation
180 survival extension indeed stemmed from *unc-58gf* expression in RIS.
181

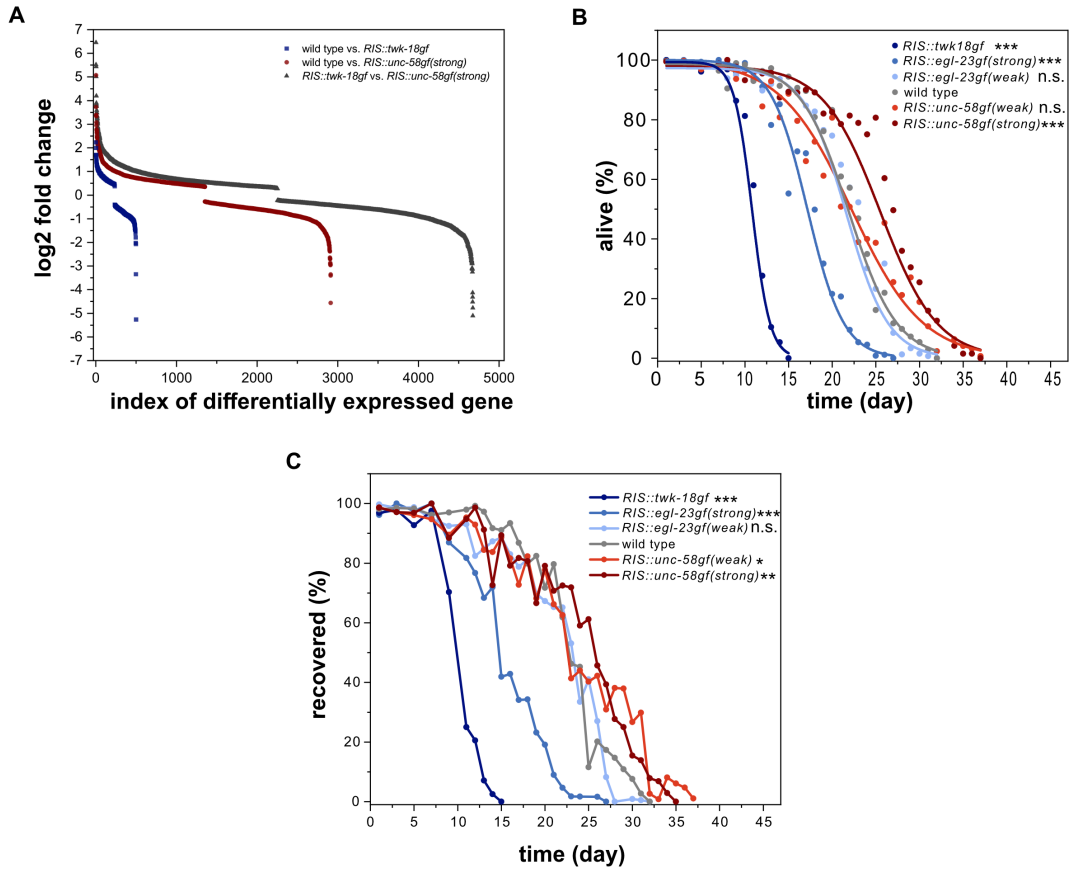

182
183 **Figure 2 – Survival of starvation-induced L1 arrest is a function of RIS activity**

184 A) *RIS::twk-18gf* and *RIS::unc-58gf(strong)* strains cause divergent transcriptional
185 profiles. Shown is the log2 fold change for all differentially expressed genes. A gene was
186 counted as differentially expressed with an FDR<0.05.
187 B) Strong inactivation significantly decreases survival in L1 arrest whereas strong
188 activation prolongs survival (three-parameter logistic fit, see also supplementary table S1,
189 Fisher's Exact Test was conducted when 50% of wild-type worms were alive (day 22)).
190 The p-values were FDR corrected with Benjamini-Hochberg procedure with a 5% false
191 discovery rate. The plot includes data from three replicates. ***p<0.001.
192 C) Recovery from L1 arrest depends on RIS activity with strong inactivation leading to a
193 reduced recovery and constant activation leading to a prolonged ability to recover. For
194 statistics, the Fisher's Exact Test was conducted at the time when 50% of wild-type
195 worms recovered (day 23). The p-values were FDR corrected with Benjamini-Hochberg
196 procedure with a 5% false discovery rate. The plot includes data from two replicates. N.s.
197 p>0.05, *p<0.05, **p<0.01, ***p<0.001. Fisher's Exact Test.
198
199
200 **Ion channel mutant expression in RIS controls baseline RIS activity**
201
202 How are RIS activity, sleep behavior and survival linked? To shed light on this question,
203 we imaged RIS calcium activity in these mutants. [10]. We used microfluidic chambers to
204 keep and image the larvae. This method allowed for a quantification of RIS baseline
205 activity, RIS calcium activation transients, and sleep behavior [37, 38]. We were able to
206 measure RIS activity for the first 12 days of starvation, and found that the effects of the
207 channel transgenes were consistent across the entire time of starvation that we analyzed
208 (Fig. 3A for two-day starvation, 3B for all time points). We first analyzed the baseline
209 activity of RIS in the absence of calcium transients. The mean RIS baseline calcium activity
210 levels were reduced by the strongly inactivating transgenes *twk-18gf* and *egl-23gf(strong)*.
211 Baseline activity levels were modestly increased by *unc-58gf(weak)* and strongly increased
212 by *unc-58gf(strong)*. The magnitude of the baseline calcium signal alterations of the
213 different transgenes were thus in accordance with the expression levels and the expected
214 strengths of the leak currents (Fig 1F). These data demonstrate that transgenic *unc-58gf*

215 can be used as a tool for increasing calcium activity in a neuron that does not normally
216 express *unc-58* [17, 31, 32]. We used these tools to create a set of strains that allows for
217 probing associations of baseline activity levels and survival as well as sleep.

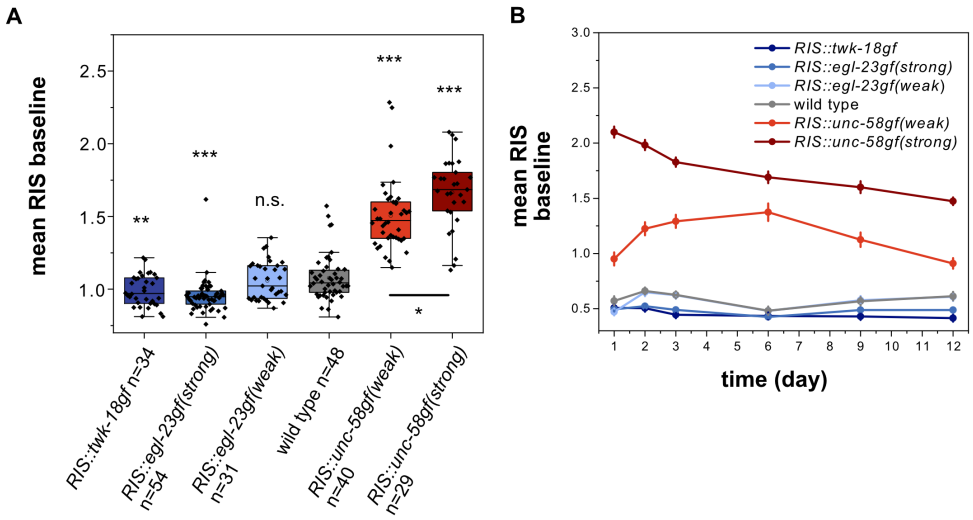

218
219
220 **Fig. 3 – Ion channel mutant expression in RIS controls baseline RIS activity**
221 A) Ion channel expression in RIS results in a dose-response strain set with varying levels
222 of RIS baseline activity. n.s. $p>0.05$, **$p<0.001$, ***$p<0.001$, Welch test with FDR
223 correction for multiple testing.
224 B) Long term RIS baseline activity for RIS activity strains from day 1 to day 12 of
225 starvation.
226
227
228 ***RIS::unc-58gf(strong)* inhibits sleep behavior during L1 arrest**
229
230 We next quantified motion quiescence as a readout for sleep and tracked mobility behavior
231 during L1 arrest inside microfluidic chambers. We used GCaMP fluorescence to quantify
232 RIS activation transients across the entire measurement [10]. Consistent with previous
233 reports [10, 12, 20], wild-type RIS showed activation transients over a constant baseline,
234 and calcium transients were accompanied by phases of behavioral quiescence (Fig 4A-G).
235 Calcium transients were completely abolished in both the strongest deactivation strains
236 (Fig 4A, B) as well as in the strong activation strain (4F). In the mild deactivation strain

237 calcium transients were still visible and correlated with behavioral quiescence, but were
238 decreased in magnitude (Fig. 4C/G, S3A). In *RIS::unc-58gf(weak)*, RIS calcium transient
239 activity and bouts of behavioral activity were increased (Fig. 4E). These results suggest
240 that RIS activation transients are required for sleep induction and that strong inactivation
241 prevents these transients. Mobility quiescence decreased with inactivation and was
242 increased with modest activation as expected. We anticipated that the elevated RIS calcium
243 baseline of *RIS::unc-58gf(strong)* might be associated with a further increase in sleep
244 behavior compared with the weak activation. Mobility quiescence was, however,
245 completely abolished by strong RIS activation in most of the animals (Fig. 4H). These
246 findings were additionally confirmed for a longer period of starvation up to day 12 (Fig.
247 4I). The loss of quiescence of the strong RIS activation strain was similar to, but not as
248 strong as in *aptf-1(-)* (Fig. S2B). The sleep amounts for each strain are consistent for several
249 days in L1 arrest (Fig. 4I). In summary, baseline RIS activity correlates with behavioral
250 quiescence over a wide range of conditions, except for the *RIS::unc-58gf(strong)*
251 transgene, which appears to cause a lack of RIS calcium transients and sleep behavior.

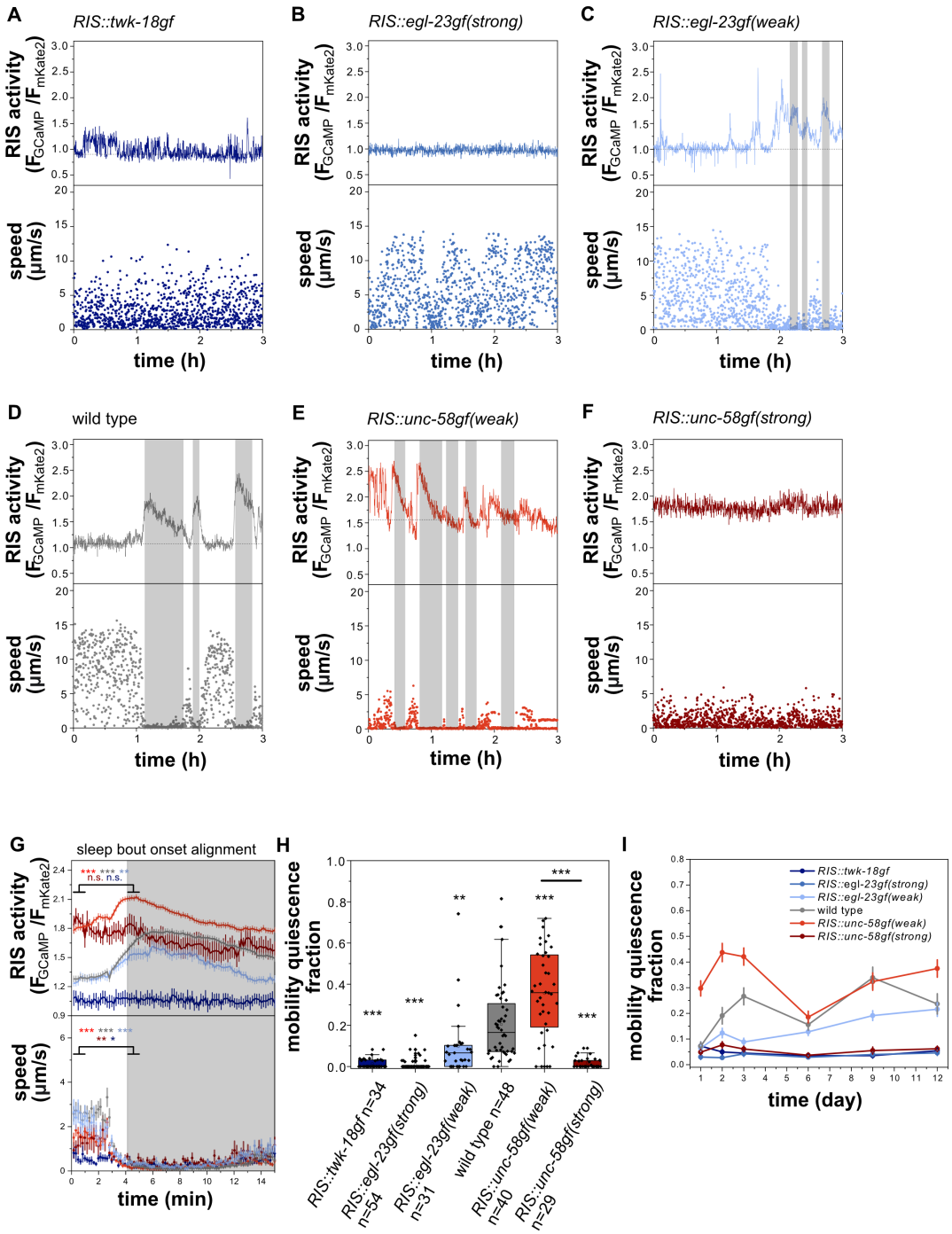

Figure 4 - Both, strong inactivation of RIS as well as *RIS::unc-58gf(strong)* prevent sleep behavior during L1 arrest

257 A-F) Ion channel expression in RIS controls calcium activity and sleep behavior.
258 Mobility quiescence bouts (grey shade) correlate with RIS transients. RIS movement
259 speed was measured. A) *RIS::twk-18gf* and B) *RIS::egl-23gf(strong)* larvae do not have
260 detectable mobility quiescence bouts or RIS transients. C) *RIS::egl-23gf(weak)* has
261 reduced mobility quiescence bouts. D) Wild-type RIS activation transients and
262 immobility bouts. E) *RIS::unc-58gf(weak)* spends more time in mobility quiescence
263 bouts. F) *RIS::unc-58gf(strong)* has no detectable mobility quiescence bouts and no RIS
264 transients but a high constant activity.
265 G) RIS activation and immobility are correlated only for the strains that also show
266 sleeping behavior. Alignment of RIS activity and speed to mobility quiescence bout
267 onset. **$p<0.01$, ***$p<0.001$, Wilcoxon signed rank test.
268 H) Mobility quiescence is a function of RIS activity levels n.s. $p>0.05$, **$p<0.001$,
269 ***$p<0.001$, Welch test with FDR correction for multiple testing.
270 I) Long-term sleep fraction for RIS activity strains from day 1 to day 12 of starvation.
271
272
273 ***RIS::unc-58gf* impairs sleep behavior during larval development and following**
274 **cellular stress in the adult**
275
276 *C. elegans* sleeps during various stages and conditions. Previous studies showed that
277 cellular stress increases adult sleep [17, 39-42]. During development, sleep is coupled to
278 the molting cycle and occurs during a period called lethargus, which coincides with
279 formation of a new cuticle [10, 43, 44]. To test whether constant RIS baseline activation is
280 also associated with a loss of behavioral quiescence during stress-induced sleep and during
281 lethargus sleep, we tested whether *RIS::unc-58gf* affects sleep behavior during L1
282 development as well as following heat stress. For testing for stress-induced sleep, we kept
283 young adult worms inside microfluidic devices and first measured baseline behavioral
284 activity at 22°C, and then exposed the animals to heat stress at 37°C for 20 minutes. We
285 then followed the behavior again after the end of the heat shock [17]. The wild type
286 immobilized during the heat shock and displayed an increase in behavioral quiescence
287 following the heat shock. The quiescence response was attenuated in all strains in which

288 RIS was manipulated. Both *unc-58gf* expressing strains showed decreased behavioral
289 quiescence. Thus, a reduction of behavioral sleep can also be caused by *RIS::unc-*
290 *58gf(weak)* (Figure 5A-G).
291
292 To test for sleep that occurs during development, we quantified behavioral quiescence of
293 *RIS::unc-58gf(strong)* during lethargus in fed L1 larvae. Behavioral quiescence of
294 *RIS::unc-58gf(strong)* was significantly reduced compared with the wild type. The loss of
295 sleep behavior in lethargus was, however, not as strong as during L1 arrest or following
296 stress-induced sleep (Figure 5H). Hence, in all the stages and conditions that we tested,
297 sleep behavior was reduced by *RIS::unc-58gf(strong)*.
298
299 We also tested whether the lack of sleep behavior in *RIS::unc-58gf(strong)* during L1 arrest
300 causes a compensatory increase in sleep when the animals resume development. For this
301 experiment, we starved larvae for 12 days and then provided them with food, which
302 allowed for a resumption of development. We then imaged sleep behavior during L1
303 lethargus in these recovered worms. There was no increase of sleep behavior in recovered
304 *RIS::unc-58gf(strong)* larvae compared with wild type (Figure S4). Thus there was no
305 indication for rebound sleep occurring at the subsequent lethargus stage in *RIS::unc-*
306 *58gf(strong)*.

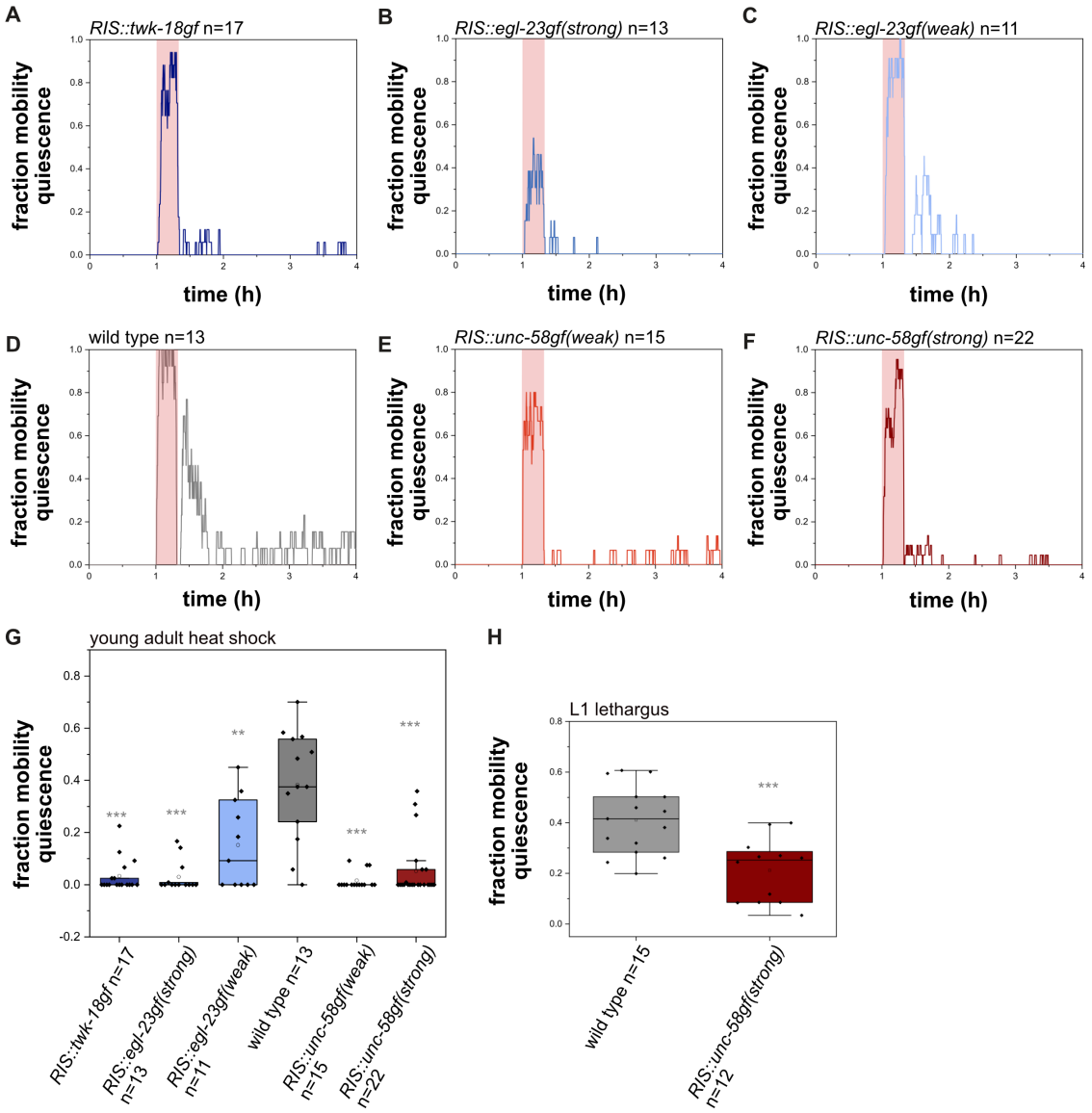

Figure 5 *RIS::unc-58gf* impairs sleep following cellular stress and during the L1 molt in developing larvae

A-F) Sleep fraction of worms of different RIS activity strains during the heat shock experiment. Animals were recorded continuously throughout the experiment. First, a 1h baseline was recorded at 22°C, then a 20min heat shock period of 37°C (in red shade) was applied, after the heat shock, the temperature was lowered to at 22°C again to monitor the response to the heat shock.

G) Quantification of time spent in sleep 20 min after the heat shock. Wild-type worms sleep on average 38.3%. All other RIS manipulations reduced quiescence. *RIS::unc-*

317 *58gf(strong)* only sleeps on average 6.5% of the time. **p<0.001, ***p<0.001, Welch test
318 with FDR correction for multiple testing.
319 H) *RIS::unc-58gf(strong)* reduces lethargus sleep compared to wild type. ***p<0.001,
320 Welch test.
321
322
323 ***RIS::unc-58gf(strong)* impairs the dampening of wake-active neuronal circuits**
324 **during L1 arrest**
325
326 *RIS::unc-58gf(strong)* caused strongly reduced sleep behavior, but the nature of the
327 residual sleep behavior in this mutant was unclear. Did the residual sleep behavior present
328 a generally weakened sleep state or a compensatory deep sleep state? To answer this
329 question, we characterized neuronal activity during in *RIS::unc-58gf(strong)* mutants. For
330 this set of experiments, we imaged larvae in microfluidic chambers and imaged neuronal
331 activity with GCaMP during L1 starvation-induced arrest.
332
333 *C. elegans* sleep is characterized as a state of globally reduced nervous system activity [12,
334 13, 20]. We measured the overall neuronal activity by utilizing a strain that expresses
335 GCaMP6s in all neurons [45]. We measured both motion behavior and overall neuronal
336 activity by extracting the calcium activity signal of all neurons as one combined signal [12,
337 22]. Consistent with previous reports, periods of behavioral quiescence were accompanied
338 by strongly reduced global neuronal activity (Fig 6A, B, S5) [12, 13, 20, 22]. We extracted
339 phases of neuronal inactivity as well as phases of behavioral inactivity from the data set.
340 In all strains, neuronal inactivity directly correlated with immobility, suggesting that
341 behavioral quiescence and neuronal quiescence are correlated in all strains irrespective of
342 the level of RIS baseline activity (Fig 6C). Thus, both behavioral inactivity and brain
343 inactivity can serve as equivalent readouts for detecting sleep in this system. Strong RIS
344 inactivation led to an increased mean overall neuronal activity of 50.7% compared to wild
345 type. Intermediate strength of inactivation did not affect mean overall neuronal activity.
346 *RIS::unc-58gf(strong)* caused a significant increase of mean overall neuronal activity of
347 35.7% (Fig 6D). These results support the notion that *RIS::unc-58gf(strong)* worms are in

348 a state of wakefulness for most of the time and lack phases of strong nervous system
349 activity dampening.

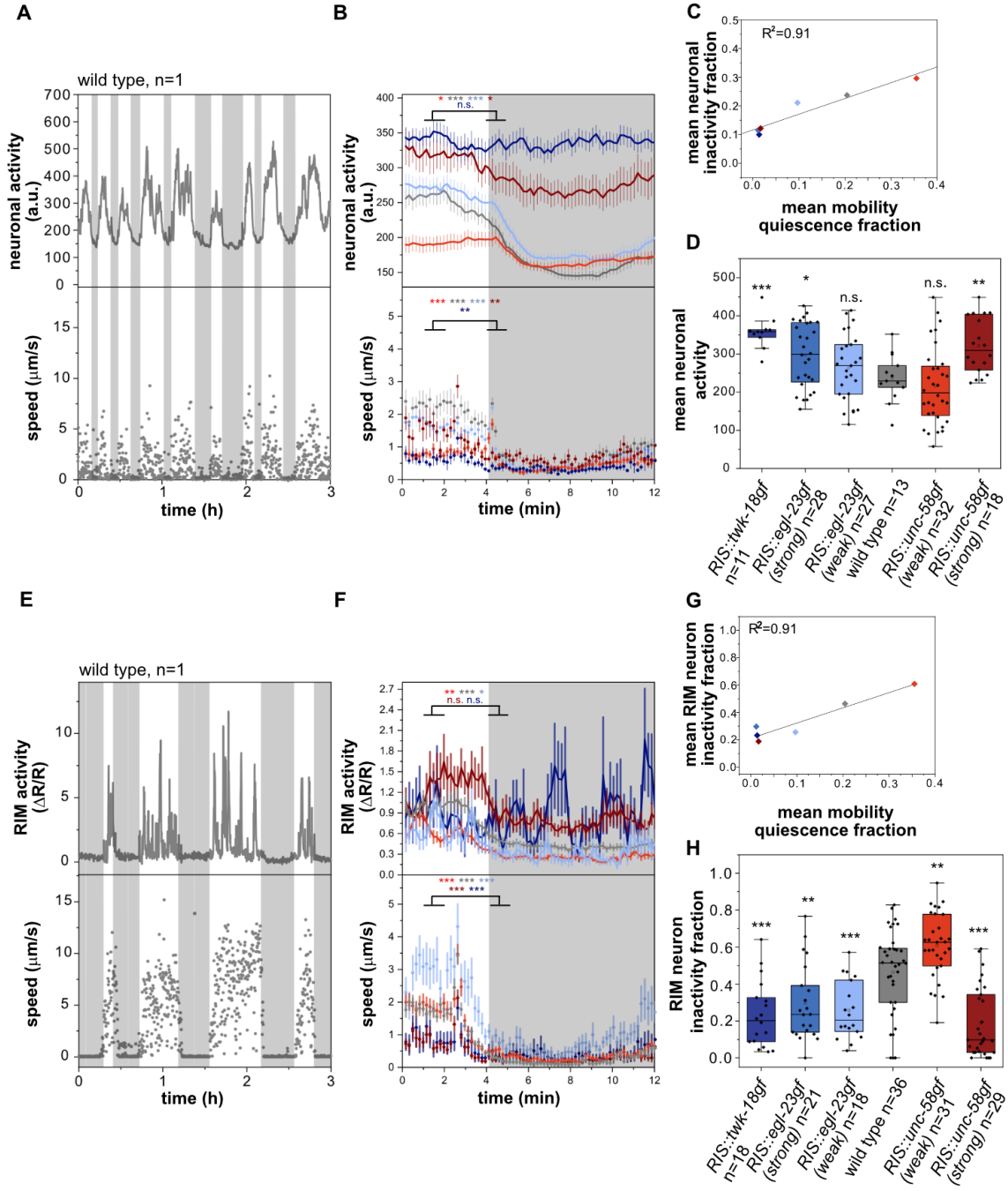

350

351 **Fig. 6 – *RIS::unc-58gf(strong)* fails to inhibit wake-active circuits**

352 A-B) Reduced global neuronal activity (grey shading) correlates with motion quiescence
353 (supplementary movies S1-S6). Head speed was measured. A) sample trace, B) alignment
354 of overall neuronal activity to mobility quiescence bout onset. ***p<0.001, Wilcoxon
355 signed rank test.
356 C) The mean neuronal inactivity fraction correlates with the mean mobility quiescence
357 fraction (linear fit) for all strains.
358 D) Strong RIS inactivation as well as *RIS::unc-58gf(strong)* caused an overall increase of
359 neuronal activity. n.s. p > 0.05, *p<0.05, **p<0.01, ***p < 0.001, Welch test with FDR
360 correction for multiple testing.
361 E-F) RIM does not activate during mobility quiescence bouts. RIM speed was measured
362 F) Sample trace (grey shade is RIM inactivity bout). Alignment of RIM activity and
363 speed to mobility quiescence bout onset. *p<0.05, **p<0.01, ***p<0.001, Wilcoxon
364 signed rank test.
365 G) The mean RIM inactivity fraction correlates with the mean mobility quiescence
366 fraction (linear fit) for all strains.
367 H) Strong RIS inactivation as well as *RIS::unc-58gf(strong)* caused an overall increase of
368 RIM activity. **p < 0.01, ***p < 0.001, Welch test with FDR correction for multiple
369 testing.
370
371
372 To characterize the effects of *RIS::unc-58gf(strong)* at the level of specific individual
373 neurons, we imaged activity of the RIM neurons, which are second layer interneurons that
374 integrate information from sensory and internal states to control motion behaviors [46, 47].
375 Again, we used GCaMP imaging in microfluidic chambers to correlate neuronal and
376 behavioral activity. RIM showed activation transients during phases of behavioral activity.
377 During phases of behavioral quiescence, RIM activity was strongly reduced and activation
378 transients were lacking (Fig 6E, F, S6). Similar to the pan-neuronal measurements, the time
379 fraction during which RIM was inactive correlated with phases of motion quiescence (Fig
380 6G). Consistent with the pan-neuronal imaging data, *RIS::unc-58gf(strong)* lacked phases
381 of RIM inactivity (Fig 6H).
382

383 An increased arousal threshold and attenuated sensory information processing are key
384 characteristics of sleep [1, 48]. In *C. elegans*, sensory information processing is inhibited
385 during sleep in developing larvae and the activity of sensory neurons is reduced [49-51].
386 For example, the mechanosensory neurons ALM and PLM display dampened activation
387 transients during sleep in developing L1 larvae [49, 50]. We measured PLM activity in
388 wild-type, *RIS::unc-58gf(strong)* and *RIS::twk-18gf* larvae. In wild-type animals, PLM
389 showed activation transients only during phases of wakefulness, whereas PLM appeared
390 to be rather inactive during sleep. In both *RIS::unc-58gf(strong)* and *RIS::twk-18gf*
391 mutants, PLM showed activation transients almost continuously throughout the time, with
392 only small episodes where PLM seemed to be not active (Figure 7). Thus, extended periods
393 of PLM neuron inactivity were absent in both *RIS::unc-58gf(strong)* and *RIS::twk-18gf*
394 mutants. Thus, *RIS::unc-58gf(strong)* inhibits the dampening of neuronal activity that is
395 associated with wakefulness behavior and thus lacks the neuronal signature of deep sleep.

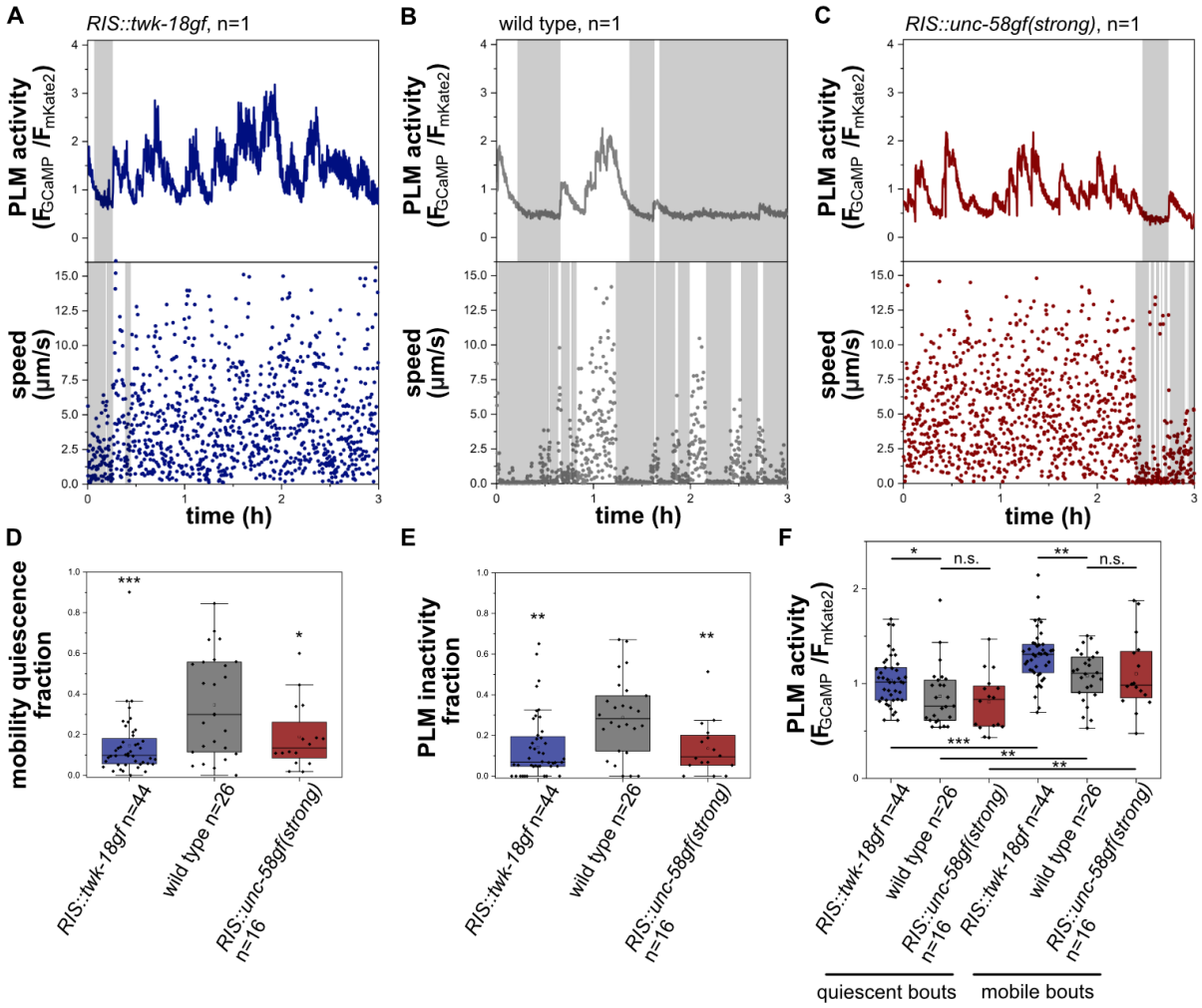

Figure 7 – Phases of sensory PLM neuron inactivity occur during sleep and are strongly reduced in *RIS::unc-58gf(strong)* and *RIS::twk-18gf*

A-C) Sample traces of PLM activity and speed in wild type, *RIS::unc-58gf(strong)* and *RIS::twk-18gf*. PLM speed was measured.

D) *RIS::twk-18gf* and *RIS::unc-58gf(strong)* reduced phases of sensory neuron quiescence. *p<0.05, *** p<0.001, Welch test.

E) *RIS::twk-18gf* and *RIS::unc-58gf(strong)* caused an overall increase of PLM activity. **p<0.01, ***p < 0.001, Welch test.

F) *RIS::twk-18gf* causes increased PLM activity in detected quiescence as well as mobility bouts. *p<0.05, **p<0.01, ***p < 0.001, Welch test for comparison between strains,

407 Wilcoxon signed rank test for comparison between the same strain quiescent and mobility
408 bouts.
409
410 ***RIS::unc-58gf(strong)* promotes muscle activity**
411
412 An absence of voluntary movement, reduced muscle contraction and a relaxed body
413 posture are hallmarks of sleep across species including *C. elegans* [44, 52-54]. If *RIS::unc-*
414 *58gf(strong)* lacks deep sleep bouts then this should be reflected by the absence of extended
415 periods of movement quiescence that coincide with reduced muscle activity. During
416 wakefulness, *C. elegans* shows locomotion behavior and feeds by contractions of the
417 pharynx muscle [55, 56]. Locomotion and pharyngeal pumping stops during sleep and the
418 animals assume a relaxed body posture [10, 44, 52, 54]. Underlying these effects, RIS
419 inhibits both locomotion and pharyngeal pumping [10, 12, 15, 57, 58]. To test the
420 hypothesis that *RIS::unc-58gf(strong)* lacks long phases of muscle relaxation that are
421 typical for sleep, we first imaged arrested larvae inside microfluidic chambers and
422 quantified more precisely movement activity of the body and the pharynx.
423
424 To quantify mobility behavior of the head and tail regions, we tracked the positions of
425 neurons that are located in these body parts. To calculate movement speed of the head, we
426 tracked the position of the RIM neurons. For tracking the tail we used the position of the
427 PLM neurons [59]. The tracking data revealed that in *RIS::twk-18gf*, both head and tail
428 movement was similar to the wild type during wakefulness. During the few quiescence
429 phases of *RIS::twk-18gf*, movement speed was reduced less than in the wild type, indicating
430 that the quiescence phases that remain in *RIS::twk-18gf* are less pronounces compared with
431 the wild type. In *RIS::unc-58gf(strong)*, head movement was slightly decreased compared
432 to wild-type worms, whereas there was no difference in tail movement (Figure 8A-B).
433 *RIS::unc-58gf(strong)* worms appeared to be more uncoordinated and the body was more
434 curved (Figure S7), which might explain the difference of head and tail movement speeds.
435 In the few locomotion quiescence phases of *RIS::unc-58gf(strong)*, there appeared to be
436 less of a reduction of movement speed.
437

438 We next imaged our transgenic strains for 1 min with a framerate of 10Hz and manually
439 scored pumping rate. This analysis revealed no significant difference in pharyngeal
440 contraction rates for all strains compared to wild type (Figure S8).
441
442 To test how *RIS::unc-58gf(strong)* and *RIS::twk-18gf* affect muscle activity, we measured
443 and quantified muscle GCaMP [52]. In the wild type, muscle calcium activity was high
444 during wakefulness, and strongly reduced during sleep. In *RIS::twk-18gf*, muscle calcium
445 was almost constantly elevated and resembled the activity levels of the wild type. *RIS::unc-*
446 *58gf(strong)* worms showed a general increase in muscle calcium activity (Figure 8C-F).
447 The increased muscle activity is consistent with and might contribute to the slightly
448 uncoordinated movement of this mutant. Phases of behavioral and muscle activity
449 dampening occurred less often, and if they occurred, then these dampened states appeared
450 to be less deep. (Figure 8G, H).

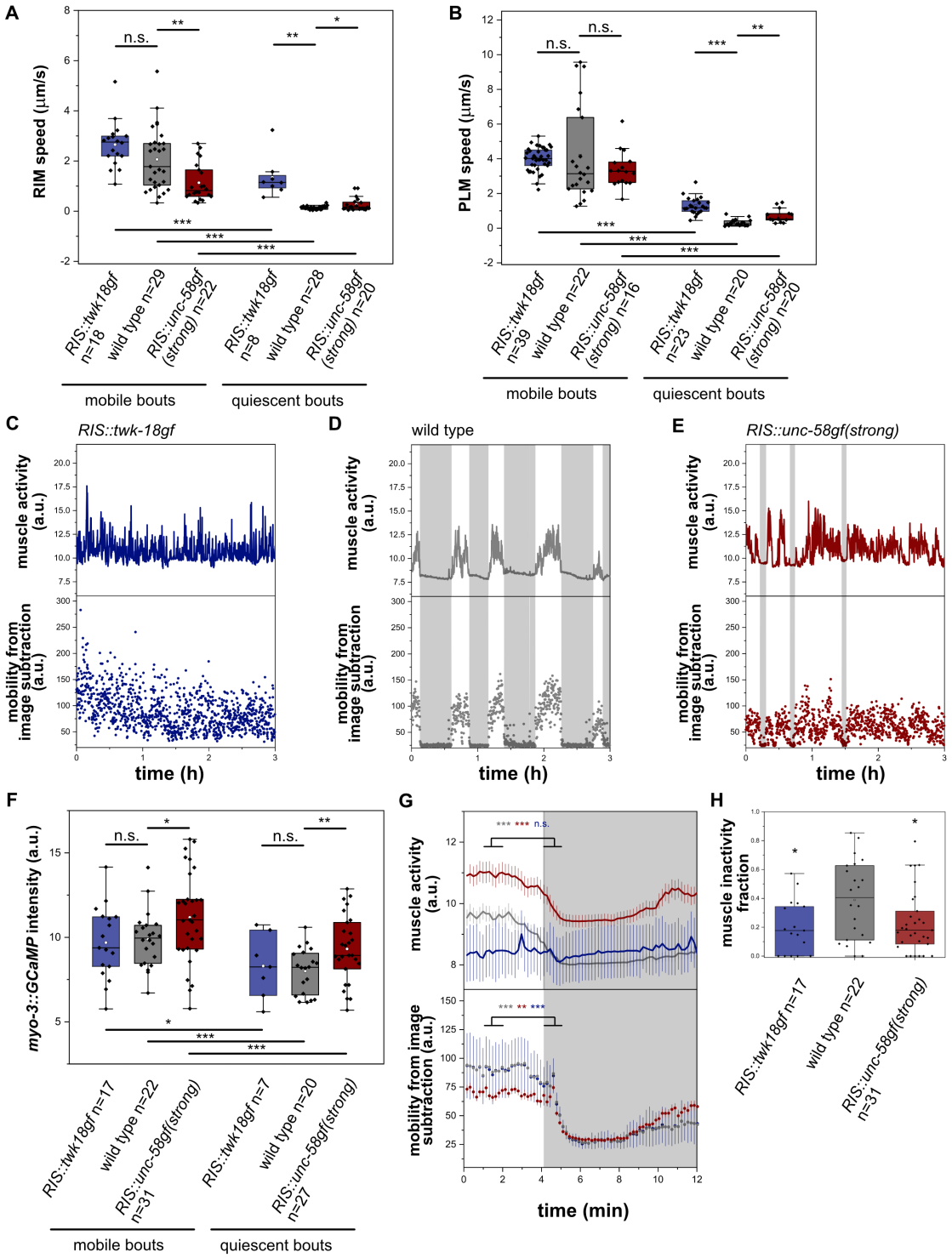

Figure 8. *RIS::unc-58gf(strong)* causes increased muscle activity.

454 A) RIM speed is reduced in *RIS::unc-58gf(strong)*. *p<0.05, **p<0.01, ***p < 0.001,
455 Welch test for comparison between strains, Wilcoxon signed rank test for comparison
456 between the same strain quiescent and mobile bouts.
457 B) PLM speed is not significantly changed in mobile bouts in *RIS::unc-58gf(strong)* and
458 increased in detected quiescent bouts. *p<0.05, **p<0.01, ***p < 0.001, Welch test for
459 comparison between strains, Wilcoxon signed rank test for comparison between the same
460 strain quiescent and mobile bouts.
461 C-E) Sample traces of muscle activity for *RIS::twk-18gf* and *RIS::unc-58gf(strong)*.
462 F) *RIS::unc-58gf(strong)* causes increased muscle activity in quiescence as well as mobility
463 bouts. *p<0.05, **p<0.01, ***p < 0.001, Welch test for comparison between strains,
464 Wilcoxon signed rank test for comparison between the same strain quiescent and mobility
465 bouts.
466 G) A sleep bout alignment reveals that *RIS::unc-58gf(strong)* has increased muscle
467 activity. **p<0.01, ***p < 0.001, Wilcoxon signed rank test.
468 H) *RIS::twk-18gf* and *RIS::unc-58gf(strong)* reduced phases of muscle inactivity.
469 *p<0.05, Welch test.
470
471
472 **In *RIS::unc-58gf(strong)*, RIS calcium activity cannot be easily elevated further by**
473 **optogenetic stimulation**
474
475 Calcium imaging suggested that the RIS baseline in *RIS::unc-58gf(strong)* is substantially
476 elevated and that calcium transients are lacking. We aimed to better understand the nature
477 of these physiological changes in RIS that are caused by expression of *RIS::unc-*
478 *58gf(strong)*. Based on the known characteristics of the *unc-58gf* mutant channel, the
479 expression of *unc-58gf* might plausibly cause a constant depolarization of the membrane
480 of RIS [32]. Depolarization in turn should lead to the activation of voltage-gated calcium
481 channels, and RIS expresses the voltage-gated calcium channels *egl-19* and *unc-2* [31].
482 The conductivity of voltage-gated calcium channels is increased by depolarization with an
483 optimum in the depolarized range. Further depolarization causes inhibition and long-term
484 stimulation reduces conductivity by desensitization [60-65]. RIS depolarization in

485 *RIS::unc-58gf(strong)* could thus perhaps be increased to allow for elevated RIS baseline
486 calcium activity, but might also inhibit further activation of calcium channel activity. We
487 tested the ability of RIS to activate by optogenetically stimulating RIS in *RIS::unc-*
488 *58gf(strong)* inside microfluidic chambers and monitored the calcium activity of this
489 neuron as well as the motion behavior of the larvae. For this experiment, we used the red-
490 shifted channelrhodopsin variant ReaChR in combination with GCaMP3 [12, 22, 57]. In
491 the wild type, optogenetic activation caused a strong increase in intracellular calcium and
492 a strong induction of motion quiescence, which is consistent with previous results [12, 15,
493 22, 57]. By contrast, optogenetic activation of RIS in *RIS::unc-58gf(strong)* did not
494 increase RIS activity further and did not induce behavioral quiescence (Fig 9A-B). This
495 result is consistent with the view that *RIS::unc-58gf(strong)* causes a heightened level of
496 RIS activity that cannot be easily increased further with optogenetic activation. Hence, in
497 *RIS::unc-58gf(strong)*, RIS appears to be locked in a state of heightened activity while
498 further activation seems to be inhibited.

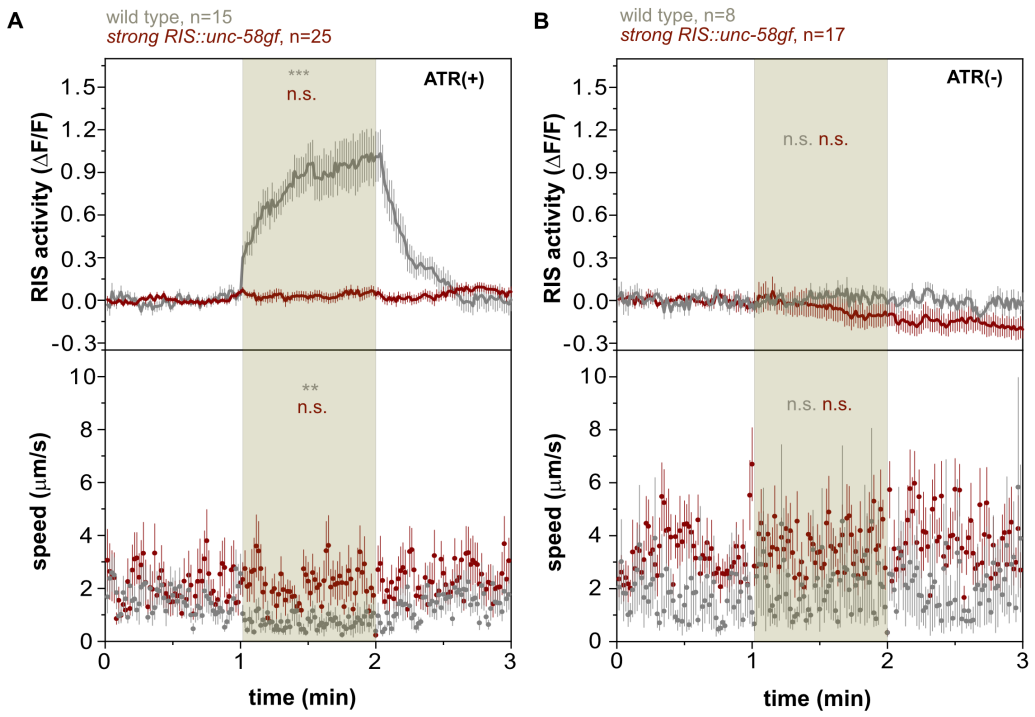

499

500

501 **Figure 9 *RIS::unc-58gf(strong)* is refractory to optogenetic activation of RIS**

502 A) Optogenetic activation of RIS during the stimulation time (minute 1-2) leads to an
503 increase of RIS activity and reduced mobility in wild-type worms but it does not affect
504 the strong RIS activation strain. RIS speed was measured. A statistical comparison was
505 made between baseline (0-1min) and stimulation (1-2min). n.s. $p>0.05$, **$p<0.01$,
506 ***$p<0.001$, Wilcoxon signed rank test.
507 B) Control for the optogenetic experiment. Without ATR treatment, neither the wild type
508 nor the strong RIS activation strain, shows a response to green light. N.s. $p>0.05$,
509 Wilcoxon signed rank test.
510
511
512 **Long-term optogenetic activation of RIS increases RIS baseline activity and inhibits**
513 **activation transients**
514
515 *RIS::unc-58gf(strong)* appears to cause increased RIS activity that cannot easily be
516 increased further. This could hypothetically be explained by a high level of depolarization
517 in *RIS::unc-58gf(strong)* that causes both RIS baseline elevation as well as inhibition of
518 RIS calcium transients. To test the idea that constant depolarization elevates baseline RIS
519 activity while inhibiting activation transients, we used long-term optogenetic activation.
520 We used again ReaChR to depolarize the membrane and followed the activity of RIS.
521 Optogenetic tools like ReaChR typically display a brief photocurrent peak activity within
522 the first second of light exposure and then plateau at a lower photocurrent level for an
523 extended period of time [66]. We previously used ReaChR to establish long-term
524 optogenetic manipulations in *C. elegans* [23]. To test for the activation of RIS during
525 prolonged optogenetic activation, we activated ReaChR in RIS with orange light for 11h
526 and followed the activity of RIS using GCaMP and measured mobility of the larvae that
527 were kept inside microfluidic chambers. During the first hour of optogenetic stimulation
528 of RIS, there was a strong increase of calcium activity as well as of behavioral quiescence
529 (Figure 10A-C). After this first peak period, the ongoing optogenetic stimulation led to
530 lower but more constant increase of RIS baseline activation (which was, however, weaker
531 than the activation observed in *RIS::unc-58gf(strong)* average calcium baseline activity
532 increase in *RIS::unc-58gf(strong)* compared with wild type was 1.55, and average calcium

533 activity baseline increase from 2-11h of activation in *RIS::ReaChR* compared with wild
534 type was 1.25) (Figure 10D, E). Long-term optogenetic activation caused reduced calcium
535 transients, and the residual calcium transients did not correlate with phases of immobility.
536 This indicates that long-term optogenetic activation has an inhibitory effect on RIS calcium
537 transients (Figure 10F). The optogenetic long-term RIS activation did not cause a
538 measurable decrease in behavioral quiescence (Figure 10C). Thus, long-term optogenetic
539 stimulation leads to a constantly increased RIS baseline activity and an inhibition of RIS
540 calcium transients that is similar to, but weaker than, the activation observed in *RIS::unc-*
541 *58gf(strong)*. This difference in effect strength might be explained by the difference in ion
542 conductivity of these channels [32, 66]. These data indicate that long-term optogenetic
543 stimulation can lead to a constant increase in baseline RIS calcium activity at a level that
544 is above the baseline activity without optogenetic stimulation, yet lower than the maximum
545 possible optogenetic RIS activation peak intensity. These optogenetic data are consistent
546 with the idea that increased depolarization of RIS leads to a constant elevation of baseline
547 calcium activity and impairs calcium transients.
548
549
550 **Long-term optogenetic activation of RIS causes a small increase in survival**
551
552 Our data using *RIS::unc-58gf(strong)* indicated that extended survival of L1 arrest is
553 associated with increased overall RIS activity. To confirm this result with an independent
554 approach, we used *RIS::ReaChR* for long-term activation of RIS using the OptoGenBox
555 system [23]. We kept L1 larvae inside microchambers and constantly stimulated the entire
556 chambers with orange light. The optogenetic stimulation was only paused briefly once
557 every day to monitor the survival of the larvae. The stimulation protocol was applied until
558 all larvae had died. Optogenetic long-term RIS activation caused a small trend for increased
559 survival (p=0.09 Logrank, p=0.02 Fisher's Exact Test), which is consistent with the view
560 that activation of RIS promotes survival. The small effect size is consistent with the small
561 RIS activity increase caused by extended optogenetic stimulation (Figure 10G). Thus, this
562 experiment is consistent with and supports the view that RIS activation promotes survival
563 of L1 arrest.

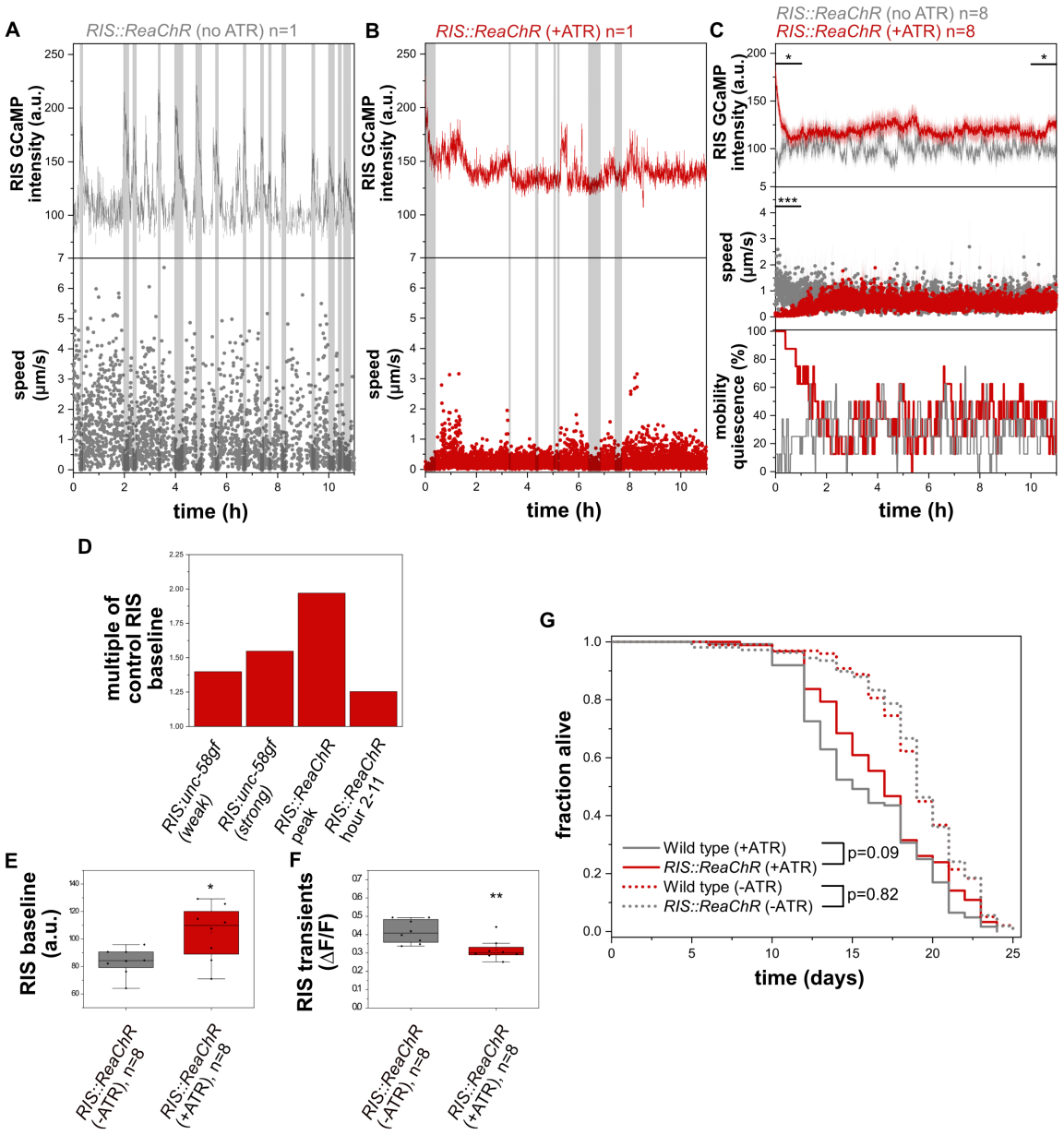

Figure 10 – Long-term optogenetic activation of RIS increases overall RIS calcium activity and promotes survival

A) Sample trace of control larvae without retinal in which RIS cannot be activated optogenetically. RIS speed was measured.

B) Long-term optogenetic RIS activation by orange light in the presence of retinal.

C) Long-term activation of RIS by ReaChR leads to an initial strong increase in calcium activity in RIS and simultaneous mobility quiescence followed by a mild RIS activity increase yet no increase in movement speed or movement quiescence.

573 D) Comparison of RIS activity level changes caused by *RIS::unc-58gf(strong)* and by
574 optogenetic activation of RIS. The data was normalized to their respective controls.
575 E) Long-term optogenetic activation of RIS significantly increases RIS baseline. *p<0.05
576 Welch test.
577 F) Transients in RIS are significantly reduced in magnitude and don't correlate with
578 quiescence. **p<0.01 Welch test.
579 G) Long-term optogenetic activation of RIS inside microfluidic chambers leads to a small
580 increase in survival (p=0.09 Logrank test, p=0.02 Fisher's Exact Test, 3 technical
581 replicates, n=92 for *RIS::ReaChR*(+ATR), n=98 *RIS::ReaChR*(-ATR), n=124 wild type
582 (+ATR), n=108 wild type (-ATR))
583
584
585 **Lethal blue-light stimulation activates RIS, and RIS supports survival of lethal blue**
586 **light**
587
588 Disturbing sleep by sensory stimulation leads to arousal that forces wakefulness and
589 prevents the dampening of underlying neuronal circuits [12, 20, 22, 44, 67, 68]. Sleep
590 disturbance or deprivation can cause increased RIS activation [22, 24, 69]. The high level
591 of RIS activity in turn could be protective under such conditions and promote survival [24].
592 Thus, *RIS::unc-58gf(strong)* might cause a state that is similar to a state caused by
593 prolonged sleep deprivation or disturbed sleep. In both, disturbed sleep and *RIS::unc-*
594 *58gf(strong)*, the activity of wakefulness circuits is not dampened yet coincides with
595 elevated RIS activity.
596
597 To further illustrate the idea that sensory stimulation activates RIS while impairing sleep,
598 we stimulated worms with a lethal intensity of blue light. We used arrested L1 larvae after
599 48h in the absence of food, a condition during which the animals normally show regular
600 RIS activation transients and sleeping behavior [12]. We kept L1 larvae in microchambers
601 and repeatedly applied pulses of blue light while monitoring RIS activity and motion
602 behavior. For comparison, we used control animals that were exposed to shorter pulses of
603 blue light of only one tenth the length, thus still allowing for calcium imaging. Control

604 larvae displayed sleeping behavior detected by motion quiescence and RIS calcium activity
605 during about a quarter of the time (Fig 11A, B). Strong blue-light stimulation caused an
606 increase in RIS calcium activity compared with control animals (after 1h of strong blue-
607 light stimulation, the activity of RIS was approximately 5.6-fold higher compared with
608 worms that were stimulated with a lower dose). Many of the calcium transients were very
609 short, however, and did not coincide with increased motion quiescence (Fig 11B-C).
610 Hence, the stronger blue-light stimulus increased RIS activity but apparently did not
611 increase sleep behavior.
612
613 To probe for the role of RIS in survival of lethal blue-light stimulation, we compared wild-
614 type and *RIS::twk-18gf* animals, in which RIS activated less under blue-light stimulation
615 (Fig 11C). We scored the time point at which the animals became terminally immobile,
616 which presents an established proxy to score for death [70]. Control animals with
617 functional RIS died around 7-8h after strong blue-light stimulus onset. RIS-impaired
618 animals already died at around 6h after stimulus onset. The presence of functional RIS
619 hence extended survival by 15% (Fig 11D).
620
621 Thus, stimulation by a lethal blue-light stimulus can increase RIS calcium activity without
622 increasing RIS-dependent sleep behavior. While all animals were eventually killed by the
623 blue-light stimulus, RIS activity slightly extended survival. The blue-light experiment thus
624 supports the idea that RIS is a protective neuron that activates upon stressful stimulation.
625 As in *RIS::ReaChR* and during long-term optogenetic stimulation of RIS, increased RIS
626 activity was not associated with increased sleep behavior.

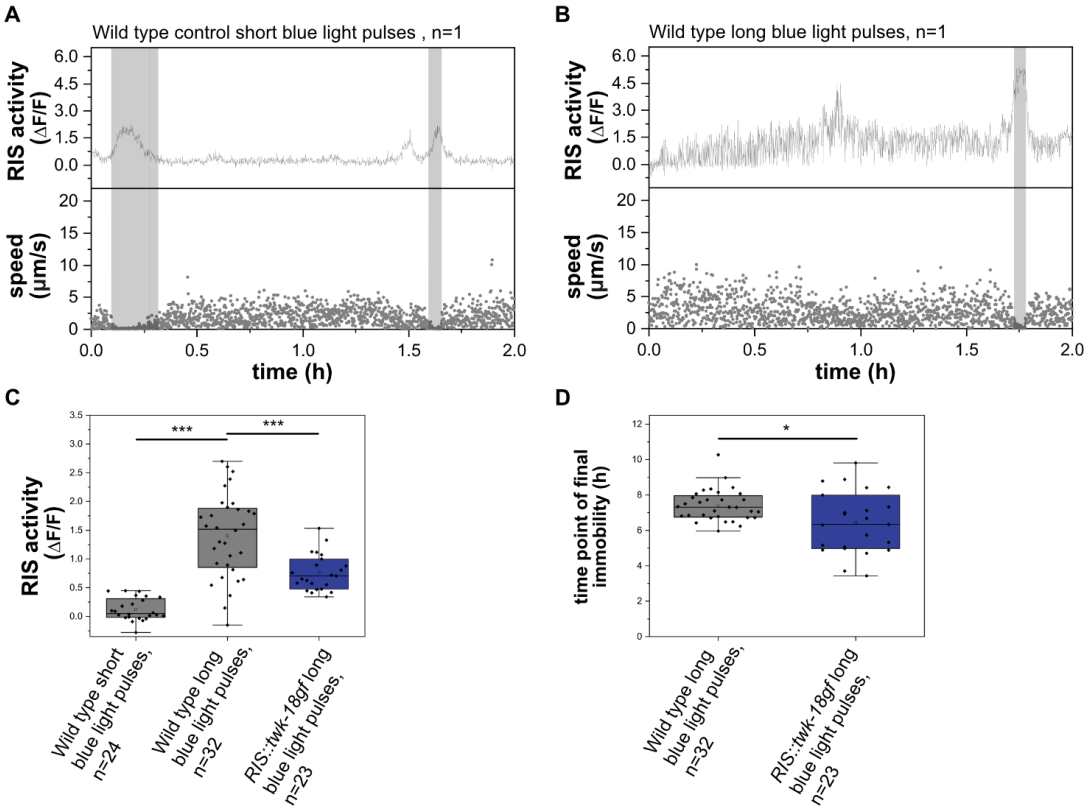

Figure 11 - RIS activates upon lethal blue-light stimulation and extends survival

A) Sample trace for a control worm stimulated by a short blue light stimulus. RIS speed was measured.

B) Sample traces of wild-type worms upon stimulation with a long blue-light stimulus. The grey shaded area presents detected time in motion quiescence.

C) The strong stimulus increased normalized RIS activity over baseline compared to control worms. ***$p<0.001$, Welch test.

D) Wild-type worms have a survival advantage over RIS-inhibited worms upon exposure to the lethal blue-light stimulus. *$p<0.05$, Welch test.

***flp-11* is a key neuropeptide gene required for quiescence behavior in L1 arrest**

What are the key transmitters that RIS uses to control sleep during L1 arrest? GABA is expressed in RIS but has not been shown to play a substantial role in promoting sleep [10,

643 15]. FLP-11 is a group of neuropeptides of RIS that present the major transmitters of RIS
644 required for sleep induction during development [11]. Expression from the *flp-11* promoter
645 depends on neuronal activity levels [71], and is increased in *RIS::unc-58gf(strong)* (Fig
646 S3B), suggesting that FLP-11 might also be a major transmitter for sleep induction during
647 L1 arrest. To directly test the role of FLP-11 in quiescence during L1 arrest, we measured
648 the effects of *flp-11* deletion (*flp-11(-)*) using microfluidic chamber imaging [11]. *flp-11(-*
649 *)* strongly reduced quiescence behavior (Fig 12A). *RIS::unc-58gf(strong)* still displayed a
650 small fraction of quiescence behavior during L1 arrest. To test whether this residual
651 quiescence was caused by *flp-11*, we deleted the entire *flp-11* gene in the *RIS::unc-*
652 *58gf(strong)* operon locus (Figure S9A) and quantified quiescence behavior. The sleep loss
653 of *RIS::unc-58gf(strong)* was reduced further by *flp-11(-),* suggesting that the residual
654 quiescence behavior in *RIS::unc-58gf* indeed depends on *flp-11* (Fig 12A).
655

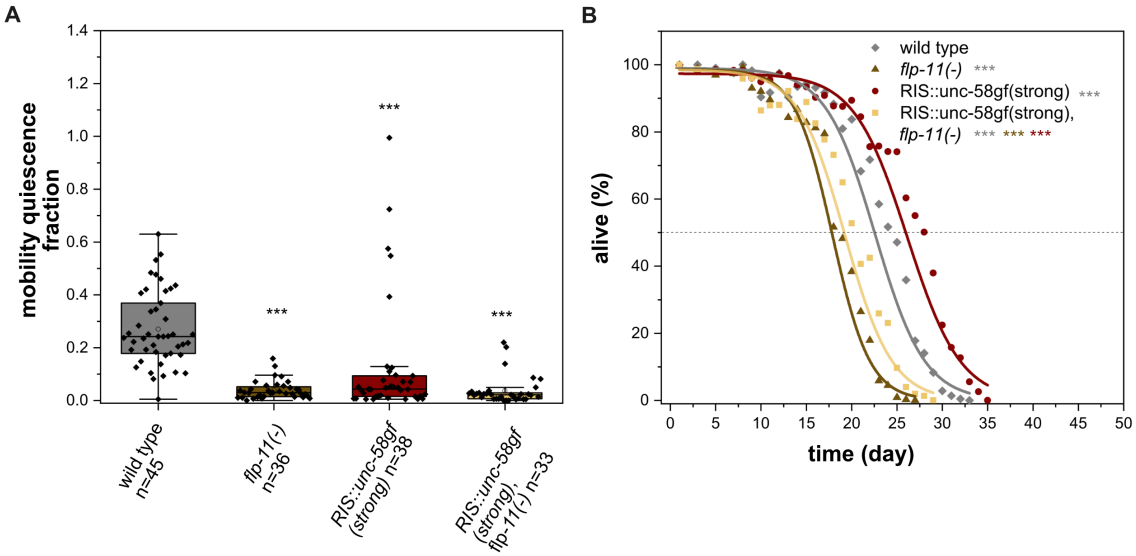

656

657 **Figure 12 – FLP-11 is required for sleep during L1 arrest**

658 A) Deletion of the neuropeptide gene *flp-11* causes loss of sleep. Immobility in *RIS::unc-*
659 *58gf(strong)* is increased when *flp-11* is deleted. ***p<0.001, Welch test with FDR
660 correction for multiple testing.

661 B) Loss of the FLP-11 neuropeptides leads to strongly reduced survival (three-parameter
662 logistic fit, see also supplementary table S1, Fisher's Exact Test was conducted on day
663 18) for comparisons when *flp-11(-)* was the shortest lived condition, day 20) when

664 *RIS::unc-58gf(strong), flp-11(-)* was the shortest lived condition or day 24) when wild
665 type was the shortest lived condition. The p-values were FDR corrected with Benjamini-
666 Hochberg procedure with a 5% false discovery rate. The plot includes data from three
667 replicates. ***p<0.001.
668
669
670 **FLP-11 neuropeptides support survival**
671
672 What is the key transmitter of RIS that promotes survival? RIS is GABAergic, but GABA
673 has been suggested to be a negative regulator of lifespan [72]. We showed above that *flp-*
674 *11* is required for most of the immobility during L1 arrest sleep. We hence tested whether
675 FLP-11 neuropeptides are also required for survival. Deletion of *flp-11* reduced survival
676 by 24.7%, suggesting that *flp-11* contributes to survival (Fig. 12B). To test whether *flp-11*
677 is required for increased survival caused by *RIS::unc-58gf(strong)*, we measured survival
678 in the *RIS::unc-58gf(strong), flp-11(-)* strain. *flp-11(-)* suppressed almost the entire
679 survival extension caused by *RIS::unc-58gf(strong)* (Fig. 12B). Similarly, the recovery
680 upon feeding was suppressed by *flp-11(-)* in *RIS::unc-58gf(strong)* (Figure S9B). Together,
681 these experiments indicate that *flp-11* plays an important role in survival and recovery of
682 L1 arrest both in the wild type and in *RIS::unc-58gf(strong)*.
683
684 These results suggest that *flp-11* plays two roles, one role is to promote sleep and the other
685 is to promote survival. Deletion of *flp-11* blunts survival less than strong RIS inactivation,
686 indicating that additional neurosecretory factors might also contribute to survival. As RIS
687 expresses multiple neuropeptides and also GABA [11, 15, 17], it may use multiple
688 transmitters to control sleep behavior and survival. In summary these data suggest that
689 FLP-11 neuropeptides are the major transmitters released by RIS to promote both sleep as
690 well as survival during L1 arrest.
691
692
693 **Discussion**
694

695 Tools to manipulate neuronal activity are instrumental for studying neuronal circuits and
696 physiology. Here we establish the constitutively active sodium channel gene *unc-58gf* as a
697 tool for activation of a neuron that normally does not express *unc-58* [31, 32]. Modest
698 expression of *unc-58gf* in RIS during L1 arrest caused an increased baseline activity of RIS
699 and increased the probability of RIS to experience calcium activation transients. It thus
700 appears that *unc-58gf* can activate RIS when expressed at lower level. Strong expression
701 of *unc-58gf* in RIS caused constant high levels of baseline RIS activity yet prevented
702 further activation transients. When expressed highly, *unc-58gf* thus locks RIS activity at a
703 level that is higher than the normal baseline and at the same time also inhibits RIS calcium
704 transients. Thus, *unc-58gf* can be used as a tool to create different and complex patterns of
705 neuronal activity, but the level of expression is crucial to achieve different effects. Together
706 with constitutively active potassium ion channels that cause various levels of inhibition,
707 activity of a neuron can be modulated from strong inhibition to constant elevation of
708 baseline activity.
709
710 RIS inhibits wakefulness neurons to cause sleep behavior and it promotes survival under
711 stressful conditions such as larval starvation or wounding [10, 12, 18, 24, 35]. A
712 parsimonious explanation linking these two observations would be that sleep promotes
713 survival, for example through energy conservation or behavioral optimization [27]. Energy
714 conservation and behavioral optimization certainly are important functions of sleep
715 behavior [28]. In addition, sleep neurons could promote physiological benefits by
716 mechanisms that do not necessarily depend on sleep behavior.
717
718 How can the manipulation of neuronal activity be employed to solve how neurons control
719 behavioral and physiological function? Here we used transgenic expression of ion channel
720 mutants in RIS to shed light on the relationship between RIS activity, sleep behavior and
721 survival. *RIS::unc-58gf(strong)* promoted survival, but also inhibited sleep behavior. Thus,
722 *RIS::unc-58gf(strong)* allowed for an uncoupling of sleep behavior and survival functions
723 of RIS. Our data thus suggest that the sleep-active RIS neuron can promote survival
724 independently of sleep.
725

726 What are hypothetical mechanisms that allow for the uncoupling of sleep behavior and
727 survival benefits of RIS? The loss of sleep behavior in *RIS::unc-58gf(strong)* could
728 hypothetically be explained by the absence of calcium transients in RIS. This could, for
729 example, be caused by desensitization of wakefulness circuits that are downstream of RIS.
730 According to this hypothesis, wakefulness circuits would decrease their activity with
731 increasing RIS activity, and would start getting more active again only after a period of
732 stagnating or decreasing RIS activity. Both, the induction of sleep behavior and the
733 promotion of survival by RIS depend on FLP-11 neuropeptides, which are thought to be
734 released upon RIS activation [11]. The two functions of FLP-11 might mechanistically
735 separate at the level of divergent receptors, signaling pathways or cell types downstream
736 of FLP-11 that mediate either the sleep or the survival response. For example, the receptors
737 and downstream cell types that mediate the effects of FLP-11 on dampening wakefulness
738 circuits might desensitize quickly, thus limiting the amount of behavioral sleep that can be
739 induced by FLP-11 released from RIS. Along these lines, RIS activity might exert a
740 survival-promoting effect through a mechanism with different desensitization properties.
741 Survival appears to be a function of RIS activity, depends on *flp-11*, but does not seem to
742 depend on activation transients. Thus, the underlying signaling components do not seem to
743 desensitize quickly but might respond to lower levels of RIS activity or might integrate
744 RIS activity over time. This could hypothetically be achieved by FLP-11 activating
745 downstream receptors and cell types that react sensitively to FLP-11 concentration, that do
746 not easily desensitize and that promote survival upon sensing FLP-11. The key FLP-11
747 receptors required for promoting sleep and survival and the cells in which these receptors
748 function have not yet been identified [11]. The identification of FLP-11 receptors will
749 allow for further studies of the mechanisms by which FLP-11 causes sleep behavior and
750 survival. Another hypothetical explanation for changes in sleep behavior upon expression
751 of ion channel mutants might be changes in the underlying neuronal connectivity. Further
752 experimentation is required to test these speculative hypotheses.
753
754 What is the mechanism and role of homeostatic compensation during sleep deprivation?
755 Homeostatic regulation can compensate for lost or disturbed sleep across species and plays
756 an important role in the regulation of sleep in *C. elegans* [22, 53, 67, 69, 73]. The typical

757 effects of disturbing sleep or depriving an animal of sleep are a reduction of sleep behavior
758 caused by continued activity of wakefulness circuits that steer behavioral activity.
759 Increased behavioral activity is often accompanied by a subsequent overactivation of sleep-
760 active neurons that promote a rebound phase of increased sleep duration or intensity.
761 Rebound sleep in turn is thought to compensate for lost or disturbed sleep, at least partially
762 [8, 22, 24, 67, 69, 73, 74].
763
764 How is *RIS::unc-58gf(strong)* related to sleep deprivation and sleep homeostasis? Does
765 *RIS::unc-58gf(strong)* trigger homeostatic compensation of the lost sleep? Does the
766 transgene cause a state that is similar to the effects of sleep-deprivation? To answer these
767 questions, we first studied behavioral sleep across stages. Across the life of arrested larvae,
768 behavioral quiescence was reduced in *RIS::unc-58gf(strong)*. Furthermore, sleep was
769 reduced by *RIS::unc-58gf(strong)* during L1 lethargus and after stress in the adult. We also
770 studied the activity of excitable cells in *RIS::unc-58gf(strong)* in arrested L1 larvae. We
771 studied the activity of sensory neurons, interneurons and body wall muscle. All of these
772 excitable cells are known to be rather inactive during sleep and thus the study of the activity
773 of these excitable cells allows for a quantitative description of sleep depth. Our data showed
774 that the sleep bouts in *RIS::unc-58gf(strong)* are less pronounced and hence appear to be
775 less deep. Hence we could not find any signs of deeper or compensatory sleep in *RIS::unc-*
776 *58gf(strong)*. By contrast, the analysis of excitable cells suggested that the residual bouts
777 of behavioral quiescence in *RIS::unc-58gf(strong)* were generally weakened. *RIS::unc-*
778 *58gf(strong)* thus displays the neuronal signature of sleep deprivation or disturbed sleep,
779 i.e. the combination of impaired wakefulness circuit dampening and over activation of RIS.
780 Thus, *RIS::unc-58gf(strong)* might be understood and employed as a model of disturbed
781 sleep or of sleep deprivation.
782
783 Does RIS activate when the animals are disturbed to promote survival [12, 18, 22, 24, 69]?
784 To further illustrate the idea of RIS acting as a promoter of survival, we disturbed animals
785 during sleep via a lethal blue-light stimulus. Lethal blue light increased RIS activity and
786 functional RIS was required for extending the survival of the animals during blue-light

787 stimulation yet did not increase sleep behavior. This supports the idea that RIS activates
788 upon sensory stimulation to promote survival independently of increasing sleep behavior.
789
790 What is the mechanism by which RIS promotes survival? Is there an important role of RIS
791 to conserve energy by shutting down behavior? The reduction of brain and muscle activity
792 likely contributes to survival by conserving energy. While energy consumption appears to
793 be playing a role in survival, behavioral activity and thus energy consumption does not
794 correlate with survival when transmission from RIS is strongly increased. In *RIS::unc-*
795 *58gf(strong)* animals, neuronal, muscle and behavioral activity are high and consume
796 energy, yet survival is increased. Hence RIS appears to be able to promote survival
797 independently of sleep behavior and despite the energy loss that can be expected to be
798 caused by the increased activity of excitable cells [28]. As both sleep and survival are
799 functions of RIS activity over a wide range of conditions, the two processes should be
800 coupled during normal sleep. During each sleep bout, RIS depolarizes and thus should
801 promote both, sleep and survival. Such coupling of sleep and survival during normal sleep
802 might ensure that phases of brain and behavioral inactivity coincide with phases during
803 which survival-promoting processes are active. Tight coupling might serve to optimize
804 energy expenditure, as energy conserved by sleep could be directly allocated to survival-
805 promoting processes [28].
806
807 How does RIS cause physiological protection and increased survival independently of
808 conserving energy? RIS promotes survival of stressful conditions and underlying changes
809 in protective gene expression [12, 18, 24]. Together with the apparent strong reduction of
810 sleep behavior in *RIS::unc-58gf(strong)*, this might suggest that the role of RIS
811 overactivation upon disturbance or sleep deprivation is not only to promote rebound sleep
812 behavior, but also to promote protective physiological benefits that support survival. An
813 important function of RIS might thus be to promote survival when the animal is disturbed
814 by sensory stimulation. Disturbance, e.g. by blue light, might directly be stressful and thus
815 require an increased survival response. Disturbed sleep is often associated with stress, for
816 example when mechanical stimuli are experienced. Hence RIS might hypothetically also

817 act as part of a sensory system that activates during stimulation to signal an increased
818 demand of physiological protection.
819
820 The FOXO transcription factor DAF-16 has been shown to be linked to the control and
821 functions of sleep. It is required for sleep under various conditions including during L1
822 arrest. Also, FOXO has been shown to be activated upon sleep deprivation during both
823 lethargus as well as during L1 arrest and to be required for increased rebound sleep
824 following sleep disturbances [24, 58, 67, 73] (Fig. S10). A plausible model hence suggests
825 that RIS activation promotes DAF-16-dependent gene expression changes in order to
826 support survival [24]. Our data indicate that RIS strongly promotes protective gene
827 expression despite the loss of sleep behavior. Thus, *RIS::unc-58gf(strong)* intensifies the
828 survival function of RIS while inhibiting the sleep function of RIS.
829
830 By controlling the activity of RIS, we showed that the survival function and the sleep
831 behavior function of this neuron can be decoupled. By constantly elevating RIS baseline
832 activity, we generated a condition in which wakefulness neural activity and sleep-active
833 neuron activity coexist. A similar condition often underlies disturbed sleep. Our data
834 suggest that when sleep is disturbed, RIS promotes survival despite the loss of behavioral
835 sleep. It would be interesting to study whether sleep neurons in other species also can
836 promote physiological benefits in the face of lost sleep.
837

838 **Materials and Methods**

839

840 **Resource and Materials Availability**

841 Key *C. elegans* lines that were used in this project are available at the Caenorhabditis
842 elegans Genetics Center. Other *C. elegans* strains, plasmids, or additional reagents
843 generated for this study are available upon reasonable request.

844

845 **Data and Code Availability**

846 Raw and processed data as well as MATLAB scripts will be made publicly available.

847

848 **Experimental model and subject details**

849 *C. elegans* hermaphrodites were maintained at 20°C. They were kept on Nematode Growth
850 Medium Plates (NGM). The *Escherichia coli* strain OP50 served as a food source during
851 maintenance [75].

852

853 **Method Details**

854

855 **Creation of transgenic animals**

856

857 **Crossing *C. elegans* strains**

858 Males were generated via heat shock or maintained by a continuation of crossings of
859 worms of the same genotype [76]. Single worms of the F2 generation were genotyped
860 using duplex PCR genotyping [77]. For crossing fluorescent transgenes, fluorescent
861 markers were used. All strains and primers of this study can be found in the
862 supplementary tables S2 and S3.

863

864 **Creating mutants with the CRISPR/Cas9 system**

865 We designed the sequences of the following transgenes in silico. Transgenes were
866 synthesized and inserted into the genome by using CRISPR/Cas9 by SunyBiotech.
867 Transgene sequences were verified by Sanger sequencing.

868

869 PHX1433 *flp-11(syb1433 [flp-11-SL2-egl-23cDNA(A383V)-linker-mKate2]) X*
870 PHX1445 *aptf-1(gk794) II; flp-11(syb1445[flp-11-SL2-unc-58(L428F)-linker-*
871 *mKate2]) X*
872 PHX1464 *flp-11(syb1464[flp-11-SL2-egl-23cDNA(L229N)-linker-mKate2]) X*
873 PHX2193 *flp-11(syb2193[flp-11b-SL2(gpd-2)-mKate2-linker-twk-18(e1913)]) X*
874 PHX2493 *lgc-38(syb2346[flp-11p::dpy-10 site::flp-11 3'UTR], syb2493[ReaChR-*
875 *linker*-mKate2]) III.
876 PHX3190 *lgc-38(syb2346[flp-11p::dpy-10 site::flp-11 3'UTR] ,syb3190[unc-*
877 *58(e665)-linker(GSGSGSGSG)-mKate2]) III*
878 PHX4110 *lgc-38(syb2346[flp-11p::dpy-10 site::flp-11 3'UTR], syb4110[unc-58gf-*
879 *CAI-1.0-linker(GSGSGSGSG)-mKate2]) III*
880 PHX4416 *aptf-1(gk794) II; flp-11(syb1445 syb4416) X*
881

882 The coding sequences of the ion channel transgenes were synthesized and consisted each
883 of the spliced coding sequence of the ion channel including the mutation that caused the
884 leak current [32], a C-terminal linker sequence followed by a C-terminal mKate2 gene. The
885 coding sequence of mKate2 was codon optimized and intronized [78]. The coding
886 sequences of the ion channels were not codon optimized to allow for proper folding of the
887 membrane proteins. We tried codon-optimization [78] of the *unc-58(L428F)* channel gene
888 and mKate2 to achieve high expression, but this also caused aggregation of the fluorescent
889 fusion protein (Fig S1A, D). Hence, we used the endogenous gene sequence for the channel
890 and only codon-optimized mKate2.

891 Analysis of the RIS transcriptome showed that *flp-11* has the strongest and most specific
892 promoter of all RIS-expressed genes, with 157-fold higher expression in RIS than in other
893 neurons [17]. *flp-11* is also expressed in other neurons, albeit at low levels [11, 17, 31].
894 Using imaging settings that cause oversaturation of the mKate2 signal in RIS revealed that
895 there is a weak expression of *unc-58gf::mKate2* in a few neurons in the ventral cord in
896 *RIS::unc-58gf(strong)* (Fig S1F). Expression from the *flp-11* promoter in RIS but not in
897 other neurons depends on *aptf-1* [11]. We hence imaged mKate2 expression in *aptf-1(-).*

898 Consistent with previous results [11], mKate2 expression was abolished in RIS but was
899 still present in the ventral cord (Fig S1G). Thus, expression from the *flp-11* promoter is
900 strong, has a high level of RIS specificity, and RIS expression depends on *aptf-1*.

901

902 The sequences of the ion channels of the strains PHX1433, PHX1445, PHX1464 and
903 PHX2193 were inserted after the stop codon of the *flp-11* endogenous coding sequence
904 together with an SL2 site. Thus, an operon was created that expressed both *flp-11* and the
905 ion channel gene from the *flp-11* promoter. The transgenes of PHX2493, PHX3190 and
906 PHX4110 were generated via a single-copy knock-in loci for defined gene expression (SKI
907 LODGE) system [34]. For the SKI LODGE expression in RIS we first inserted the minimal
908 *flp-11* 3' and 5'UTRs separated by a *dpy-10* sgRNA cutting site. The expression from these
909 minimal UTR sequences allowed specific expression in RIS, but the expression levels were
910 lower compared with the endogenous *flp-11* locus (Fig 1A-D, S1A-D). The final sequences
911 of all transgenes can be found in the supplementary Text S1.

912

913 **Imaging**

914

915 **Microfluidic devices**

916 Worms were filmed in microfluidic devices made from agarose hydrogel as previously
917 described [37, 38]. In brief, a PDMS mold was used to cast box-shaped indentations from
918 melted 5% agarose diluted in M9 buffer. After agarose hydrogel solidification the stamp
919 was removed resulting in hundreds of microchambers sized 110x110x10µm for L1 arrest
920 chambers or 190x190x15µm for L1 lethargus chambers per agarose slab. Depending on
921 the experiment, approximately 9-36 pretzel-stage eggs per strain were then transferred
922 without food for L1 arrest or with food for lethargus into the indentations in the hydrogel
923 and the chambers were closed with a coverslip and kept in a temperature-controlled dish.
924 Hatching of the larvae in the absence of food caused L1 arrest. Chambers were timed so
925 that the worms were incubated for 48h at 25°C before imaging. The number of biological
926 replicates (n) imaged in microfluidic devices is stated in each figure. One or several
927 technical replicates (different microfluidic devices) were imaged for each experiment.

928

929 **Software**

930 All image acquisition was performed with Nikon NIS Elements 5 software (Nikon,
931 Tokyo).

932

933 **Dark Differential Contrast (DIC) Imaging**

934 Long-term dark differential contrast (DIC) images were acquired with a standard 100W
935 halogen lamp and an infrared filter (Semrock Brightline HC 785/62) (Idex Health and
936 Science, New York). The images for L1 arrest imaging were taken 48h upon starvation for
937 12h with a frame rate of 0.1Hz. A 20x objective for imaging was combined with a 0.7 lens.
938 Lethargus data was acquired with similar settings except the frame rate was 0.2Hz.

939

940 **Functional Ca^{2+}-imaging**

941 For calcium imaging we used either a back-illuminated sCMOS camera (Photometrics
942 Prime 95B, 1200x1200 pixels) (Figure 3, 4, 8C-H, S3) or an Andor iXon EMCCD camera
943 (512x512 pixels, Andor Technology Ltd., Belfast). (Figure 6, 7, 8A-B S5, S6). The gain of
944 the iXon camera was set to 200. The iXon camera's read out mode was 10MHz at 14-bit.
945 The images of the Photometrics camera were binned 2 x 2.

946

947 A 20x objective was used to simultaneously image 3 x 3 adjacent microchambers
948 containing one worm each (This configuration was used to obtain data for Figures 6, 7, 8A-
949 B, S5, S6). A 10x objective combined with a 1.5x lens was used to simultaneously image
950 6 x 6 adjacent microchambers containing one worm each (this configuration was used to
951 obtain data for Figures 3, 4, 8C-H, S3).

952

953 For calcium imaging we utilized a 480nm LED and a standard GFP filter set (EGFP,
954 Chroma). The EMCCD camera TTL signal triggered the LED. The 490nm intensities were
955 set to either 0.23mW/mm^2 with an exposure time of 50ms (Figure 3A, 4A-H, 8C-H),
956 0.33mW/mm^2 (Figure 6A-D) or 0.51 mW/mm^2 (Figure 6E-H), both with an exposure time
957 of 5ms or 0.33mW/mm^2 with an exposure time of 10ms (PLM). Additional mKate2
958 fluorescence images were acquired for the RIS, RIM and PLM activity experiments. For

959 this measurement we used a 585nm LED and a set of standard Texas Red filters (Chroma).
960 The 585nm LED intensity was set to 0.11mW/mm^2 while imaging with a 50ms exposure
961 time (RIS) and to 0.15 mW/mm^2 for acquiring images with a 100ms exposure time (RIM,
962 PLM). Calcium and mKate2 imaging were carried out with a frame rate of 0.1Hz for 3h.
963 As the ion channels were additionally tagged with an mKate2, the parental strains without
964 the GCaMP/mKate2 construct were imaged with the same settings with the 585nm LED.
965 Here, no signal could be observed in the parental strains.
966
967 For the long-term calcium imaging from day 1 to day 12 we utilized slightly different LED
968 light intensities. Here, the 490nm intensity was set to 0.34mW/mm^2 and the 585nm light
969 had an intensity of 0.21mW/mm^2.
970
971 **Optogenetic activation**
972 For optogenetic RIS activation experiments, the agarose containing the microchambers
973 was supplemented with 10µl of 10mM all-trans-retinal (ATR, Sigma Aldrich) dissolved in
974 ethanol 1h before the start of image acquisition. In experiment in Figure 9, A baseline of
975 GCaMP images was recorded for 1min with a frame rate of 0.33Hz. This was followed by
976 a stimulation phase of 1min, in which again GCaMP images were acquired with a frame
977 rate of 0.33Hz. In between the camera exposures, the worms were illuminated with 585nm
978 LED light with an intensity of 0.17mW/mm^2 for 800ms triggered by the software. After
979 the stimulation period, a recovery period of 1min was imaged, in which GCaMP images
980 were acquired with a frame rate of 0.33Hz. The 490nm LED intensities for imaging were
981 set to 0.39mW/mm^2 and images were acquired with an exposure time of 5ms.
982
983 For the long-term optogenetic imaging worms (Fig 10), a stimulation phase of 11h was
984 recorded in which GCaMP images were acquired with a frame rate of 0.33Hz. In between
985 the camera exposures, the worms were illuminated with 585nm LED light with an intensity
986 of 0.17mW/mm^2 for 800ms triggered by the software.
987
988 **Expression of mKate2 of the RIS activity strains**

989 Larvae were synchronized via bleaching [17] and hatched in M9 buffer at 25°C. Imaging
990 of most strains was performed after 48h in the L1 arrest stage by transferring worms with
991 a 10 µl liquid drop onto an agarose pad (5% agarose solved in M9 buffer). The *RIS::unc-*
992 *58gf and flp-11(-)* worms were imaged 24h after bleaching. Larvae were then fixed through
993 the addition of 10 µl of 25mM levamisole (Sigma Aldrich).
994
995 To image the expression levels of the different RIS activity transgenes, mKate2 was
996 imaged with an Andor Revolution disc system (Andor Technology Ltd.) and a CSU-X1
997 spinning disc head (Yokogawa). The 561nm laser light intensity was set to 0.49mW/mm^2.
998 The worms were imaged through a 100x oil objective and by an Andor iXon Ultra EMCCD
999 camera (1024x1024 pixels) (Andor Technology Ltd., Belfast). An EM gain of 200 was
1000 included and the camera read-out time was set to 30MHz. A z-stack of 21planes, each
1001 0.5µm apart (10µm in total) was acquired. For comparison, a maximum z-stack projection
1002 was calculated.
1003
1004 **Image analysis**
1005
1006 **DIC images analysis**
1007 Mobility of worms was analyzed from DIC images though image subtraction [79]. The
1008 matrix of intensity values of the preceding image was subtracted from the matrix of
1009 intensity of the following image. A mean of all values of the difference matrix was then
1010 calculated to attain a mean smoothed image subtraction value, which represents the
1011 movement of the worm.
1012
1013 To identify lethargus in fed worms, the non-pumping time prior to molting was identified.
1014 For the sleep analysis in recovery lethargus after 12 days of starvation followed by
1015 refeeding, 3h prior to molt were analyzed for mobility quiescence.
1016
1017 **Analyzing functional Ca^{2+}-images**
1018 Neuronal intensities were automatically analyzed via custom-written MATLAB scripts.
1019 These codes extracted the regions of interest through an intensity threshold and acquired

1020 the intensities and position data. The extracted regions were set to be slightly bigger than
1021 the actual size of the neuron to allow for background intensity detection and background
1022 subtraction. The pan-neuronal activity was measured treating the head neurons as a
1023 combined signal. The RIS GCaMP activity in Figure 6 was determined by extracting the
1024 position data of the corresponding mKate2 signal. A larger region of interest was extracted
1025 and a fitting percentage of that was calculated as the signal. The extracted position data of
1026 the signal served to calculate the speed values.
1027
1028 RIS, RIM and PLM activities were normalized by dividing GCaMP intensities through
1029 corresponding mKate2 intensities. In the optogenetic experiment, the baseline
1030 measurements were used for normalization.
1031
1032 **Mobility quiescence detection**
1033 First, speeds or image subtraction mean intensities were smoothed over 30 time points
1034 through the *smooth* function in MATLAB, which is a first-degree polynomial local
1035 regression model. Smoothed speeds and image subtraction values were normalized
1036 between 0 and 1 for each individual animal with 0 being the lowest speed value and 1 the
1037 highest speed value the animal possessed. A mobility quiescence bout was counted when
1038 the normalized speed was below a specific percentage for a certain amount of time. For
1039 calcium imaging experiments with the 20x objective (Figure 6), the normalized speed had
1040 to be below 10% for at least 3min. The RIS activity experiment, which was filmed with a
1041 10x objective, required a percentage threshold of 5% for a minimum of 4min. For DIC
1042 images filmed with the 20x objective, the normalized mean image subtraction values had
1043 to be below 15% for at least 3min to be counted as sleep time points.
1044
1045 **Mobility quiescence bout onset alignment**
1046 Speeds and GCaMP intensities were aligned to the start of mobility quiescence bouts,
1047 which had been detected by the mobility quiescence bout analysis. Mobility quiescence
1048 bouts were only counted for the alignment when the worm was mobile throughout 3min
1049 prior to the mobility quiescence bout onset. This alignment was carried out with a custom-
1050 written MATLAB script.

1051

1052 **Neuronal inactivity detection**

1053 The neuronal activities were treated similarly as speed values for the mobility quiescence
1054 detection. The nervous system was counted as inactive when it was below 20% of the
1055 smoothed and normalized activity for at least 3min.

1056

1057 **RIM neuron inactivity detection**

1058 RIM peaks were detected through custom-written MATLAB scripts. First, the activity
1059 values were smoothed using the inbuilt *smooth* function over 5 time points. Then, peaks of
1060 a minimum prominence of 0.2 were extracted via the inbuilt function *islocalmax.* RIM was
1061 counted as inactive when there were no detected peaks for at least 5min.

1062

1063 **Induction of cellular stress by heat shock**

1064 The heat shock was carried out following a previously described protocol and utilizing a
1065 previously described heat shock device [17]. To summarize, young adult worms were
1066 imaged in 370x370x45µm microfluidic chambers and for a total of 4h. 5 to 12 worms were
1067 transferred from plates grown at 20°C to the microchamber. The worms were starved for
1068 90min at 20°C before filming. During the entire duration of the movie, DIC images were
1069 acquired at a frequency of 0.1Hz. First, a baseline was recorded for 1h with the sample
1070 holder temperature set to 22°C and the heating lid set to 25°C. Then the heat shock was
1071 conducted with the sample holder temperature set to 37°C and the heating lid set to 39°C
1072 for 20 minutes. Finally, a recovery phase was recorded with the sample holder temperature
1073 set to 22°C and the heating lid set to 25°C for 2h 40min.

1074

1075 **Pumping assay**

1076 Worms were imaged in 110x110x10µm microfluidic chambers. DIC images were
1077 acquired with a frequency of 10 Hz for 1min. Pumps of the grinder were then counted
1078 manually with the help of a clicker.

1079

1080 **Survival assay in liquid culture**

1081 RIS impairment has been shown to confer a reduction of survival in both liquid culture and
1082 in microfluidic chambers [12, 23, 24, 36]. Worms were synchronized by bleaching [17]. 3-
1083 4 days before bleaching, 10-12 L4 stage worms were transferred onto NGM plates with a
1084 diameter of 6cm. 1-2 plates were bleached per strain and the day of bleaching was defined
1085 as day 0. The worms were kept in 1ml of M9 buffer in 1.5ml Eppendorf tubes in a rotator
1086 at 20°C for most survival assays. The following day was counted as day 1 of the lifespan.
1087 During the survival assay, the worms were kept in liquid culture in 1ml M9 buffer in 2ml
1088 Eppendorf tubes. This resulted in a population density of approximately 100 worms per
1089 10µl. The tubes were placed in a rotator at 20°C, which rotated at 20rpm. For counting,
1090 10µl drops of the liquid culture were pipetted onto fresh NGM plates for each strain
1091 respectively. The worms were allowed to recover for at least 2h after pipetting before
1092 counting. Counting was performed manually with the assistance of a clicker. The recovery
1093 number, i.e., the number of worms that developed into at least the L4 stage, was counted
1094 3-5 days after pipetting. Around 50-100 worms were counted for each strain of each
1095 replicate on each time point.
1096
1097 **Survival assay in the OptoGenBox**
1098 For the long-term optogenetic survival assay worms were kept in microfluidic chambers
1099 (110x110x15µm) as described above. Between 27 and 43 worms were used for each strain
1100 per agarose slab each containing many microfluidic chambers. A maximum of one worm
1101 was placed per microfluidic chamber. Three replicates were performed per condition. For
1102 the optogenetic activation 10µl of 10mM all-trans-retinal (ATR, Sigma Aldrich) dissolved
1103 in ethanol was added every 3-4 days. 20µl of 10µg/ml nystatin dissolved in DMSO was
1104 added 3-4 times throughout the lifespan to prevent fungal contamination. To prevent drying
1105 out of the agarose, 20µl of sterile water was added every 2 days. In the first week, the
1106 worms were counted every second day, then the survival was counted every day until all
1107 worms had died. A worm was counted as dead if a 2 min blue-light stimulus did not cause
1108 a visible behavioral response.
1109
1110 For long-term optogenetic activation of RIS, worms were placed in the OptoGenBox [23]
1111 and continuously illuminated with 10mW at 20°C.

1112

1113 **Blue light survival assay**

1114 For the blue-light survival assays worms were imaged in 110x110x10µm microchambers.
1115 A blue light stimulus of 0.74mW/mm^2 was given for 1s every 5s while simultaneously
1116 taking a GCaMP image. For the control, the same intensity stimulus was given for only
1117 100ms through the camera exposure time.

1118

1119 **Images of growing worms**

1120 The images of growing plates were taken at a Leica M125 stereomicroscope. A Jenoptik
1121 ProgRes MF captured the images utilizing the corresponding software ProgResCapturePro
1122 2.10.0.1.

1123

1124 **RNA sequencing data**

1125 RNA sequencing data is described in [24].

1126

1127 **Fitting**

1128 Origin software was used for the regression analyses. A linear regression was fitted to the
1129 data in Figure 6C and 6G. R^2 values can be found in the corresponding figures. The exact
1130 functions are in Table 1.

1131

Figure panel	fit	function
6C	linear	$y = 0.116 + 0.5494x$
6G	linear	$y = 0.21203 + 1.10949x$

1132 Table 1. Calculated functions for the regressions.

1133

1134 **Quantification and Statistical Analysis**

1135 The experimenter was blind to the genotype information during the lifespan experiments.
1136 All other experiments relied on an automated analysis and hence were not blinded. The
1137 Wilcoxon signed rank test was utilized for the comparison of speeds and GCaMP
1138 intensities within the same strain. The Welch test was conducted to compare data from
1139 different strains. The survival assay experiments were statistically analyzed by utilizing the

1140 Fisher's exact test at 50% survival of the wild type. Experiments with four or more
1141 genotypes were FDR corrected by the Benjamini-Hochberg procedure with a 5% false
1142 discovery rate. The graphs depict the mean and standard error of the mean. Box plots
1143 display individual data points, the interquartile range and the median. The whiskers
1144 represent the 10-90th percentile. A table listing all exact p-values can be found in the
1145 supplemental information (Table S4).
1146

1147 **Acknowledgements**
1148 Some strains were provided by the CGC, which is funded by NIH Office of Research
1149 Infrastructure Programs (P40 OD010440). The CRISPR strains were generated by
1150 SunyBiotech based on our design. We thank Thomas Boulin for communicating the sodium
1151 permeability of *unc-58gf* and suggesting its use as a tool for neuronal activation. This work
1152 was supported by a European Research Council Starting Grant (ID: 637860,
1153 SLEEPCONTROL).
1154

1155 **Author contributions**
1156 I.B. designed, executed and analyzed all experiments. H.B. conceived the overall structure
1157 of the study, designed the transgenes, acquired funding and supervised the project. All
1158 authors wrote the paper.
1159

1160 **Declaration of Interest**
1161 The authors declare no competing interests.

1162 **References**

1163

1164 1. Campbell SS, Tobler I. Animal sleep: a review of sleep duration across
1165 phylogeny. Neurosci Biobehav Rev. 1984;8(3):269-300. Epub 1984/01/01. PubMed
1166 PMID: 6504414.
1167 2. Diekelmann S, Born J. The memory function of sleep. Nature reviews
1168 Neuroscience. 2010;11(2):114-26. Epub 2010/01/05. doi: 10.1038/nrn2762. PubMed
1169 PMID: 20046194.
1170 3. Krueger JM, Frank MG, Wisor JP, Roy S. Sleep function: Toward elucidating an
1171 enigma. Sleep medicine reviews. 2016;28:46-54. Epub 2015/10/09. doi:
1172 10.1016/j.smrv.2015.08.005. PubMed PMID: 26447948; PubMed Central PMCID:
1173 PMC4769986.
1174 4. Anafi RC, Kayser MS, Raizen DM. Exploring phylogeny to find the function of
1175 sleep. Nature reviews Neuroscience. 2019;20(2):109-16. Epub 2018/12/24. doi:
1176 10.1038/s41583-018-0098-9. PubMed PMID: 30573905.
1177 5. Hublin C, Partinen M, Koskenvuo M, Kaprio J. Sleep and mortality: a population-
1178 based 22-year follow-up study. Sleep. 2007;30(10):1245-53. Epub 2007/11/01. doi:
1179 10.1093/sleep/30.10.1245. PubMed PMID: 17969458; PubMed Central PMCID:
1180 PMCPMC2266277.
1181 6. Van Cauter E, Spiegel K, Tasali E, Leproult R. Metabolic consequences of sleep
1182 and sleep loss. Sleep Med. 2008;9 Suppl 1:S23-8. Epub 2008/12/17. doi: 10.1016/S1389-
1183 9457(08)70013-3. PubMed PMID: 18929315; PubMed Central PMCID:
1184 PMCPMC4444051.
1185 7. Irwin MR. Why sleep is important for health: a psychoneuroimmunology
1186 perspective. Annu Rev Psychol. 2015;66:143-72. Epub 2014/07/26. doi:
1187 10.1146/annurev-psych-010213-115205. PubMed PMID: 25061767; PubMed Central
1188 PMCID: PMCPMC4961463.
1189 8. Saper CB, Fuller PM, Pedersen NP, Lu J, Scammell TE. Sleep state switching.
1190 Neuron. 2010;68(6):1023-42. Epub 2010/12/22. doi: 10.1016/j.neuron.2010.11.032.
1191 PubMed PMID: 21172606; PubMed Central PMCID: PMC3026325.
1192 9. Bringmann H. Sleep-Active Neurons: Conserved Motors of Sleep. Genetics.
1193 2018;208(4):1279-89. Epub 2018/04/06. doi: 10.1534/genetics.117.300521. PubMed
1194 PMID: 29618588; PubMed Central PMCID: PMC5887131.
1195 10. Turek M, Lewandrowski I, Bringmann H. An AP2 transcription factor is required
1196 for a sleep-active neuron to induce sleep-like quiescence in C. elegans. Curr Biol.
1197 2013;23(22):2215-23. Epub 2013/11/05. doi: 10.1016/j.cub.2013.09.028. PubMed PMID:
1198 24184105.
1199 11. Turek M, Besseling J, Spies JP, Konig S, Bringmann H. Sleep-active neuron
1200 specification and sleep induction require FLP-11 neuropeptides to systemically induce
1201 sleep. eLife. 2016;5. Epub 2016/03/08. doi: 10.7554/eLife.12499. PubMed PMID:
1202 26949257; PubMed Central PMCID: PMC4805538.
1203 12. Wu Y, Masurat F, Preis J, Bringmann H. Sleep Counteracts Aging Phenotypes to
1204 Survive Starvation-Induced Developmental Arrest in C. elegans. Curr Biol.
1205 2018;28(22):3610-24 e8. Epub 2018/11/13. doi: 10.1016/j.cub.2018.10.009. PubMed
1206 PMID: 30416057; PubMed Central PMCID: PMCPMC6264389.

1207 13. Skora S, Mende F, Zimmer M. Energy Scarcity Promotes a Brain-wide Sleep
1208 State Modulated by Insulin Signaling in C. elegans. Cell reports. 2018;22(4):953-66.
1209 Epub 2018/02/02. doi: 10.1016/j.celrep.2017.12.091. PubMed PMID: 29386137.
1210 14. Gonzales DL, Zhou J, Fan B, Robinson JT. A microfluidic-induced C. elegans
1211 sleep state. Nat Commun. 2019;10(1):5035. Epub 2019/11/07. doi: 10.1038/s41467-019-
1212 13008-5. PubMed PMID: 31695031.
1213 15. Steuer Costa W, Van der Auwera P, Glock C, Liewald JF, Bach M, Schuler C, et
1214 al. A GABAergic and peptidergic sleep neuron as a locomotion stop neuron with
1215 compartmentalized Ca2+ dynamics. Nat Commun. 2019;10(1):4095. Epub 2019/09/12.
1216 doi: 10.1038/s41467-019-12098-5. PubMed PMID: 31506439.
1217 16. Grubbs JJ, Lopes LE, van der Linden AM, Raizen DM. A salt-induced kinase is
1218 required for the metabolic regulation of sleep. PLoS biology. 2020;18(4):e3000220. Epub
1219 20200421. doi: 10.1371/journal.pbio.3000220. PubMed PMID: 32315298; PubMed
1220 Central PMCID: PMCPMC7173979.
1221 17. Konietzka J, Fritz M, Spiri S, McWhirter R, Leha A, Palumbos S, et al. Epidermal
1222 Growth Factor Signaling Promotes Sleep through a Combined Series and Parallel Neural
1223 Circuit. Curr Biol. 2020;30(1):1-16 e3. Epub 2019/12/17. doi:
1224 10.1016/j.cub.2019.10.048. PubMed PMID: 31839447.
1225 18. Sinner MP, Masurat F, Ewbank JJ, Pujol N, Bringmann H. Innate Immunity
1226 Promotes Sleep through Epidermal Antimicrobial Peptides. Curr Biol. 2021;31(3):564-77
1227 e12. Epub 2020/12/02. doi: 10.1016/j.cub.2020.10.076. PubMed PMID: 33259791.
1228 19. Makino M, Ulzii E, Shirasaki R, Kim J, You YJ. Regulation of Satiety
1229 Quiescence by Neuropeptide Signaling in Caenorhabditis elegans. Front Neurosci.
1230 2021;15:678590. Epub 2021/08/03. doi: 10.3389/fnins.2021.678590. PubMed PMID:
1231 34335159; PubMed Central PMCID: PMCPMC8319666.
1232 20. Nichols ALA, Eichler T, Latham R, Zimmer M. A global brain state underlies C.
1233 elegans sleep behavior. Science. 2017;356(6344). Epub 2017/06/24. doi:
1234 10.1126/science.aam6851. PubMed PMID: 28642382.
1235 21. Xu Y, Zhang L, Liu Y, Topalidou I, Hassinan C, Ailion M, et al. Dopamine
1236 receptor DOP-1 engages a sleep pathway to modulate swimming in C. elegans. iScience.
1237 2021;24(4):102247. Epub 2021/04/03. doi: 10.1016/j.isci.2021.102247. PubMed PMID:
1238 33796839; PubMed Central PMCID: PMCPMC7995527.
1239 22. Maluck E, Busack I, Besseling J, Masurat F, Turek M, Busch KE, et al. A wake-
1240 active locomotion circuit depolarizes a sleep-active neuron to switch on sleep. PLoS
1241 biology. 2020;18(2):e3000361. Epub 2020/02/23. doi: 10.1371/journal.pbio.3000361.
1242 PubMed PMID: 32078631.
1243 23. Busack I, Jordan F, Sapir P, Bringmann H. The OptoGenBox - a device for long-
1244 term optogenetics in C. elegans. J Neurogenet. 2020:1-9. Epub 2020/06/17. doi:
1245 10.1080/01677063.2020.1776709. PubMed PMID: 32543249.
1246 24. Koutsoumparis A, Welp LM, Wulf A, Urlaub H, Meierhofer D, Börno S, et al.
1247 Sleep neuron depolarization promotes protective gene expression changes and FOXO
1248 activation. Current Biology. 2022. doi: https://doi.org/10.1016/j.cub.2022.04.012.
1249 25. Kenyon CJ. The genetics of ageing. Nature. 2010;464(7288):504-12. Epub
1250 2010/03/26. doi: 10.1038/nature08980. PubMed PMID: 20336132.
1251 26. Baugh LR, Hu PJ. Starvation Responses Throughout the Caenorhabditis elegans
1252 Life Cycle. Genetics. 2020;216(4):837-78. Epub 2020/12/04. doi:

1253 10.1534/genetics.120.303565. PubMed PMID: 33268389; PubMed Central PMCID:
1254 PMCPMC7768255.
1255 27. Siegel JM. Sleep viewed as a state of adaptive inactivity. Nature reviews
1256 Neuroscience. 2009;10(10):747-53. Epub 2009/08/06. doi: 10.1038/nrn2697. PubMed
1257 PMID: 19654581.
1258 28. Schmidt MH. The energy allocation function of sleep: a unifying theory of sleep,
1259 torpor, and continuous wakefulness. Neurosci Biobehav Rev. 2014;47:122-53. Epub
1260 2014/08/15. doi: 10.1016/j.neubiorev.2014.08.001. PubMed PMID: 25117535.
1261 29. Krause AJ, Simon EB, Mander BA, Greer SM, Saletin JM, Goldstein-Piekarski
1262 AN, et al. The sleep-deprived human brain. Nature reviews Neuroscience.
1263 2017;18(7):404-18. Epub 2017/05/19. doi: 10.1038/nrn.2017.55. PubMed PMID:
1264 28515433.
1265 30. Klinzing JG, Niethard N, Born J. Mechanisms of systems memory consolidation
1266 during sleep. Nat Neurosci. 2019;22(10):1598-610. Epub 2019/08/28. doi:
1267 10.1038/s41593-019-0467-3. PubMed PMID: 31451802.
1268 31. Taylor SR, Santpere G, Weinreb A, Barrett A, Reilly MB, Xu C, et al. Molecular
1269 topography of an entire nervous system. Cell. 2021. Epub 2021/07/09. doi:
1270 10.1016/j.cell.2021.06.023. PubMed PMID: 34237253.
1271 32. Ben Soussia I, El Mouridi S, Kang D, Leclercq-Blondel A, Khoubza L, Tardy P,
1272 et al. Mutation of a single residue promotes gating of vertebrate and invertebrate two-
1273 pore domain potassium channels. Nat Commun. 2019;10(1):787. Epub 2019/02/17. doi:
1274 10.1038/s41467-019-08710-3. PubMed PMID: 30770809; PubMed Central PMCID:
1275 PMCPMC6377628.
1276 33. Kunkel MT, Johnstone DB, Thomas JH, Salkoff L. Mutants of a temperature-
1277 sensitive two-P domain potassium channel. J Neurosci. 2000;20(20):7517-24. doi:
1278 10.1523/JNEUROSCI.20-20-07517.2000. PubMed PMID: 11027209; PubMed Central
1279 PMCID: PMCPMC6772866.
1280 34. Silva-Garcia CG, Lanjuin A, Heintz C, Dutta S, Clark NM, Mair WB. Single-
1281 Copy Knock-In Loci for Defined Gene Expression in Caenorhabditis elegans. G3
1282 (Bethesda). 2019;9(7):2195-8. Epub 2019/05/09. doi: 10.1534/g3.119.400314. PubMed
1283 PMID: 31064766; PubMed Central PMCID: PMCPMC6643881.
1284 35. Bringmann H. Genetic sleep deprivation: using sleep mutants to study sleep
1285 functions. EMBO Rep. 2019;20(3). Epub 2019/02/26. doi: 10.15252/embr.201846807.
1286 PubMed PMID: 30804011; PubMed Central PMCID: PMCPMC6399599.
1287 36. Roux AE, Langhans K, Huynh W, Kenyon C. Reversible Age-Related
1288 Phenotypes Induced during Larval Quiescence in C. elegans. Cell Metab.
1289 2016;23(6):1113-26. Epub 2016/06/16. doi: 10.1016/j.cmet.2016.05.024. PubMed PMID:
1290 27304510.
1291 37. Bringmann H. Agarose hydrogel microcompartments for imaging sleep- and
1292 wake-like behavior and nervous system development in Caenorhabditis elegans larvae. J
1293 Neurosci Methods. 2011;201(1):78-88. Epub 2011/08/02. doi: S0165-0270(11)00418-3
1294 [pii]10.1016/j.jneumeth.2011.07.013. PubMed PMID: 21801751.
1295 38. Turek M, Besseling J, Bringmann H. Agarose Microchambers for Long-term
1296 Calcium Imaging of Caenorhabditis elegans. Journal of visualized experiments : JoVE.
1297 2015;(100):e52742. Epub 2015/07/02. doi: 10.3791/52742. PubMed PMID: 26132740;
1298 PubMed Central PMCID: PMC4544933.

1299 39. Van Buskirk C, Sternberg PW. Epidermal growth factor signaling induces
1300 behavioral quiescence in Caenorhabditis elegans. Nat Neurosci. 2007;10(10):1300-7.
1301 Epub 2007/09/25. doi: 10.1038/nn1981. PubMed PMID: 17891142.
1302 40. Hill AJ, Mansfield R, Lopez JM, Raizen DM, Van Buskirk C. Cellular stress
1303 induces a protective sleep-like state in C. elegans. Curr Biol. 2014;24(20):2399-405.
1304 Epub 2014/09/30. doi: 10.1016/j.cub.2014.08.040. PubMed PMID: 25264259; PubMed
1305 Central PMCID: PMC4254280.
1306 41. Nelson MD, Lee KH, Churgin MA, Hill AJ, Van Buskirk C, Fang-Yen C, et al.
1307 FMRFamide-like FLP-13 neuropeptides promote quiescence following heat stress in
1308 Caenorhabditis elegans. Curr Biol. 2014;24(20):2406-10. Epub 2014/09/30. doi:
1309 10.1016/j.cub.2014.08.037. PubMed PMID: 25264253; PubMed Central PMCID:
1310 PMC4254296.
1311 42. Iannacone MJ, Beets I, Lopes LE, Churgin MA, Fang-Yen C, Nelson MD, et al.
1312 The RFamide receptor DMSR-1 regulates stress-induced sleep in C. elegans. eLife.
1313 2017;6. Epub 2017/01/18. doi: 10.7554/eLife.19837. PubMed PMID: 28094002; PubMed
1314 Central PMCID: PMCPMC5241116.
1315 43. Cassada RC, Russell RL. The dauerlarva, a post-embryonic developmental variant
1316 of the nematode Caenorhabditis elegans. Dev Biol. 1975;46(2):326-42. Epub 1975/10/01.
1317 doi: 0012-1606(75)90109-8 [pii]. PubMed PMID: 1183723.
1318 44. Raizen DM, Zimmerman JE, Maycock MH, Ta UD, You YJ, Sundaram MV, et
1319 al. Lethargus is a Caenorhabditis elegans sleep-like state. Nature. 2008;451(7178):569-
1320 72. Epub 2008/01/11. doi: nature06535 [pii]10.1038/nature06535. PubMed PMID:
1321 18185515.
1322 45. Yemini E, Lin A, Nejatbakhsh A, Varol E, Sun R, Mena GE, et al. NeuroPAL: A
1323 Multicolor Atlas for Whole-Brain Neuronal Identification in C. elegans. Cell.
1324 2021;184(1):272-88 e11. Epub 2020/12/31. doi: 10.1016/j.cell.2020.12.012. PubMed
1325 PMID: 33378642.
1326 46. Piggott BJ, Liu J, Feng Z, Wescott SA, Xu XZ. The neural circuits and synaptic
1327 mechanisms underlying motor initiation in C. elegans. Cell. 2011;147(4):922-33. Epub
1328 2011/11/15. doi: 10.1016/j.cell.2011.08.053. PubMed PMID: 22078887; PubMed Central
1329 PMCID: PMC3233480.
1330 47. Li W, Kang L, Piggott BJ, Feng Z, Xu XZ. The neural circuits and sensory
1331 channels mediating harsh touch sensation in Caenorhabditis elegans. Nat Commun.
1332 2011;2:315. Epub 2011/05/19. doi: 10.1038/ncomms1308. PubMed PMID: 21587232;
1333 PubMed Central PMCID: PMC3098610.
1334 48. McCormick DA, Bal T. Sensory gating mechanisms of the thalamus. Curr Opin
1335 Neurobiol. 1994;4(4):550-6. doi: 10.1016/0959-4388(94)90056-6. PubMed PMID:
1336 7812144.
1337 49. Schwarz J, Lewandrowski I, Bringmann H. Reduced activity of a sensory neuron
1338 during a sleep-like state in Caenorhabditis elegans. Curr Biol. 2011;21(24):R983-4. Epub
1339 2011/12/24. doi: S0960-9822(11)01207-3[pii]10.1016/j.cub.2011.10.046. PubMed
1340 PMID: 22192827.
1341 50. Schwarz J, Bringmann H. Reduced sleep-like quiescence in both hyperactive and
1342 hypoactive mutants of the Galphaq Gene egl-30 during lethargus in Caenorhabditis
1343 elegans. PLoS One. 2013;8(9):e75853. Epub 2013/09/28. doi:

1344 10.1371/journal.pone.0075853. PubMed PMID: 24073282; PubMed Central PMCID:
1345 PMC3779211.
1346 51. Cho JY, Sternberg PW. Multilevel modulation of a sensory motor circuit during
1347 C. elegans sleep and arousal. Cell. 2014;156(1-2):249-60. Epub 2014/01/21. doi:
1348 10.1016/j.cell.2013.11.036. PubMed PMID: 24439380; PubMed Central PMCID:
1349 PMC3962823.
1350 52. Schwarz J, Spies JP, Bringmann H. Reduced muscle contraction and a relaxed
1351 posture during sleep-like Lethargus. Worm. 2012;1(1):12-4. Epub 2012/01/01. doi:
1352 10.4161/worm.19499. PubMed PMID: 24058817; PubMed Central PMCID:
1353 PMC3670164.
1354 53. Iwanir S, Tramm N, Nagy S, Wright C, Ish D, Biron D. The microarchitecture of
1355 C. elegans behavior during lethargus: homeostatic bout dynamics, a typical body posture,
1356 and regulation by a central neuron. sleep. 2013;36(3):385-95. Epub 2013/03/02. doi:
1357 10.5665/sleep.2456. PubMed PMID: 23449971; PubMed Central PMCID: PMC3571756.
1358 54. Tramm N, Oppenheimer N, Nagy S, Efrati E, Biron D. Why do sleeping
1359 nematodes adopt a hockey-stick-like posture? PLoS One. 2014;9(7):e101162. Epub
1360 2014/07/16. doi: 10.1371/journal.pone.0101162. PubMed PMID: 25025212; PubMed
1361 Central PMCID: PMC4099128.
1362 55. Schwartz HT. A protocol describing pharynx counts and a review of other assays
1363 of apoptotic cell death in the nematode worm Caenorhabditis elegans. Nature protocols.
1364 2007;2(3):705-14. doi: 10.1038/nprot.2007.93. PubMed PMID: 17406633.
1365 56. Song BM, Avery L. The pharynx of the nematode C. elegans: A model system for
1366 the study of motor control. Worm. 2013;2(1):e21833. doi: 10.4161/worm.21833. PubMed
1367 PMID: 24058858; PubMed Central PMCID: PMCPMC3670459.
1368 57. Urmersbach B, Besseling J, Spies JP, Bringmann H. Automated analysis of sleep
1369 control via a single neuron active at sleep onset in C. elegans. Genesis. 2016;54(4):212-9.
1370 Epub 2016/02/03. doi: 10.1002/dvg.22924. PubMed PMID: 26833569.
1371 58. Bennett HL, Khoruzhik Y, Hayden D, Huang H, Sanders J, Walsh MB, et al.
1372 Normal sleep bouts are not essential for C. elegans survival and FoxO is important for
1373 compensatory changes in sleep. BMC neuroscience. 2018;19(1):10. Epub 2018/03/11.
1374 doi: 10.1186/s12868-018-0408-1. PubMed PMID: 29523076.
1375 59. White JG, Southgate E, Thomson JN, Brenner S. The structure of the nervous
1376 system of the nematode Caenorhabditis elegans. Philos Trans R Soc Lond B Biol Sci.
1377 1986;314(1165):1-340. Epub 1986/11/12. PubMed PMID: 22462104.
1378 60. Schafer WR, Kenyon CJ. A calcium-channel homologue required for adaptation
1379 to dopamine and serotonin in Caenorhabditis elegans. Nature. 1995;375(6526):73-8.
1380 Epub 1995/05/04. doi: 10.1038/375073a0. PubMed PMID: 7723846.
1381 61. Lee RY, Lobel L, Hengartner M, Horvitz HR, Avery L. Mutations in the alpha1
1382 subunit of an L-type voltage-activated Ca2+ channel cause myotonia in Caenorhabditis
1383 elegans. EMBO J. 1997;16(20):6066-76. Epub 1997/10/08. doi:
1384 10.1093/emboj/16.20.6066. PubMed PMID: 9321386.
1385 62. Mathews EA, Garcia E, Santi CM, Mullen GP, Thacker C, Moerman DG, et al.
1386 Critical residues of the Caenorhabditis elegans unc-2 voltage-gated calcium channel that
1387 affect behavioral and physiological properties. J Neurosci. 2003;23(16):6537-45. doi:
1388 10.1523/JNEUROSCI.23-16-06537.2003. PubMed PMID: 12878695; PubMed Central
1389 PMCID: PMCPMC6740628.

1390 63. Laine V, Frokjaer-Jensen C, Couchoux H, Jospin M. The alpha1 subunit EGL-19,
1391 the alpha2/delta subunit UNC-36, and the beta subunit CCB-1 underlie voltage-
1392 dependent calcium currents in Caenorhabditis elegans striated muscle. The Journal of
1393 biological chemistry. 2011;286(42):36180-7. Epub 2011/09/01. doi:
1394 10.1074/jbc.M111.256149. PubMed PMID: 21878625; PubMed Central PMCID:
1395 PMC3196126.
1396 64. Schuler C, Fischer E, Shaltiel L, Steuer Costa W, Gottschalk A. Arrhythmogenic
1397 effects of mutated L-type Ca 2+-channels on an optogenetically paced muscular pump in
1398 Caenorhabditis elegans. Sci Rep. 2015;5:14427. Epub 20150924. doi:
1399 10.1038/srep14427. PubMed PMID: 26399900; PubMed Central PMCID:
1400 PMCPMC4585839.
1401 65. Huang YC, Pirri JK, Rayes D, Gao S, Mulcahy B, Grant J, et al. Gain-of-function
1402 mutations in the UNC-2/CaV2alpha channel lead to excitation-dominant synaptic
1403 transmission in Caenorhabditis elegans. eLife. 2019;8. Epub 20190805. doi:
1404 10.7554/eLife.45905. PubMed PMID: 31364988; PubMed Central PMCID:
1405 PMCPMC6713474.
1406 66. Lin JY, Knutsen PM, Muller A, Kleinfeld D, Tsien RY. ReaChR: a red-shifted
1407 variant of channelrhodopsin enables deep transcranial optogenetic excitation. Nat
1408 Neurosci. 2013;16(10):1499-508. Epub 2013/09/03. doi: 10.1038/nn.3502. PubMed
1409 PMID: 23995068; PubMed Central PMCID: PMC3793847.
1410 67. Driver RJ, Lamb AL, Wyner AJ, Raizen DM. DAF-16/FOXO Regulates
1411 Homeostasis of Essential Sleep-like Behavior during Larval Transitions in C. elegans.
1412 Curr Biol. 2013;23(6):501-6. Epub 2013/03/13. doi: 10.1016/j.cub.2013.02.009. PubMed
1413 PMID: 23477722.
1414 68. Choi S, Chatzigeorgiou M, Taylor KP, Schafer WR, Kaplan JM. Analysis of
1415 NPR-1 reveals a circuit mechanism for behavioral quiescence in C. elegans. Neuron.
1416 2013;78(5):869-80. Epub 2013/06/15. doi: 10.1016/j.neuron.2013.04.002. PubMed
1417 PMID: 23764289; PubMed Central PMCID: PMC3683153.
1418 69. Spies J, Bringmann H. Automated detection and manipulation of sleep in C.
1419 elegans reveals depolarization of a sleep-active neuron during mechanical stimulation-
1420 induced sleep deprivation. Sci Rep. 2018;8(1):9732. Epub 2018/06/29. doi:
1421 10.1038/s41598-018-28095-5. PubMed PMID: 29950594.
1422 70. Stroustrup N, Ulmschneider BE, Nash ZM, Lopez-Moyado IF, Apfeld J, Fontana
1423 W. The Caenorhabditis elegans Lifespan Machine. Nat Methods. 2013;10(7):665-70.
1424 Epub 20130512. doi: 10.1038/nmeth.2475. PubMed PMID: 23666410; PubMed Central
1425 PMCID: PMCPMC3865717.
1426 71. Laurent P, Soltesz Z, Nelson GM, Chen C, Arellano-Carbajal F, Levy E, et al.
1427 Decoding a neural circuit controlling global animal state in C. elegans. eLife. 2015;4.
1428 Epub 20150311. doi: 10.7554/eLife.04241. PubMed PMID: 25760081; PubMed Central
1429 PMCID: PMCPMC4440410.
1430 72. Chun L, Gong J, Yuan F, Zhang B, Liu H, Zheng T, et al. Metabotropic GABA
1431 signalling modulates longevity in C. elegans. Nat Commun. 2015;6:8828. Epub
1432 20151105. doi: 10.1038/ncomms9828. PubMed PMID: 26537867; PubMed Central
1433 PMCID: PMCPMC4667614.
1434 73. Nagy S, Tramm N, Sanders J, Iwanir S, Shirley IA, Levine E, et al. Homeostasis
1435 in C. elegans sleep is characterized by two behaviorally and genetically distinct

1436 mechanisms. eLife. 2014;3:e04380. Epub 2014/12/05. doi: 10.7554/eLife.04380.
1437 PubMed PMID: 25474127; PubMed Central PMCID: PMC4273442.
1438 74. Alam MA, Kumar S, McGinty D, Alam MN, Szymusiak R. Neuronal activity in
1439 the preoptic hypothalamus during sleep deprivation and recovery sleep. J Neurophysiol.
1440 2014;111(2):287-99. Epub 2013/11/01. doi: 10.1152/jn.00504.2013. PubMed PMID:
1441 24174649; PubMed Central PMCID: PMC3921380.
1442 75. Brenner S. The genetics of Caenorhabditis elegans. Genetics. 1974;77(1):71-94.
1443 Epub 1974/05/01. PubMed PMID: 4366476.
1444 76. Stiernagle T. Maintenance of C. elegans. WormBook. 2006:1-11. Epub
1445 2007/12/01. doi: 10.1895/wormbook.1.101.1. PubMed PMID: 18050451.
1446 77. Ahringer A. Reverse genetics. WormBook, ed The C elegans Research
1447 Community. 2006. doi: doi/10.1895/wormbook.1.47.1.
1448 78. Redemann S, Schloissnig S, Ernst S, Pozniakowsky A, Ayloo S, Hyman AA, et
1449 al. Codon adaptation-based control of protein expression in C. elegans. Nat Methods.
1450 2011;8(3):250-2. Epub 2011/02/01. doi: nmeth.1565 [pii]10.1038/nmeth.1565. PubMed
1451 PMID: 21278743.
1452 79. Nagy S, Raizen DM, Biron D. Measurements of behavioral quiescence in
1453 Caenorhabditis elegans. Methods. 2014. Epub 2014/03/20. doi:
1454 10.1016/j.ymeth.2014.03.009. PubMed PMID: 24642199.
1455

1456